IMPACT TESTING OF BRITTLE MATERIALS USING SPLIT HOPKINSON PRESSURE BAR TECHNIQUE

BY

SYED IFTEKHAR MAHMOOD

A Thesis Presented to the

DEANSHIP OF GRADUATE STUDIES

KING FAHD UNIVERSITY OF PETROLEUM & MINERALS

DHAHRAN, SAUDI ARABIA

In Partial Fulfillment of the
Requirements for the Degree of

MASTER OF SCIENCE

In

Mechanical Engineering

January 2004

KING FAHD UNIVERSITY OF PETROLEUM AND MINERALS
DHAHRAN 31261, SAUDI ARABIA

DEANSHIP OF GRADUATE STUDIES

This thesis, written by **SYED IFTEKHAR MAHMOOD** under the direction of his Thesis Advisor and approved by his Thesis Committee, has been presented to and accepted by the Dean of Graduate Studies, in partial fulfillment of the requirements for the degree of MASTER OF SCIENCE IN MECHANICAL ENGINEERING.

Thesis Committee

Prof. A.M. Eleiche (Chairman)

Dr. A.F.M. Arif (Member)

Dr. Ibrahim M. Allam (Member)

Dr. Al-Sulaiman, Faleh A.
Department Chairman

Prof. Osama A. Jannadi
Dean of Graduate Studies

10/4/04
Date

Dedicated to

My Beloved Parents & Brother

ACKNOWLEDGEMENTS

First and foremost, all praise to Almighty Allah, who alone made this accomplishment possible. Acknowledgments are due to King Fahd University of Petroleum and Minerals for the support in carrying out this research.

My heartfelt appreciation and special thanks goes to thesis advisor Prof. Abdel Salam M. Eleiche for his untiring guidance, remarkable assistance and continuous support throughout the course of this research. Working with him was an opportunity of great learning and experience. Thanks are also due to my thesis committee members, Dr. Abul Fazal M. Arif and Dr. Ibrahim M. Allam for providing valuable suggestions, help and assistance throughout the course of this work.

I also appreciate the assistance and encouragement received from the Chairman, faculty members and graduate students of the department.

My appreciation also goes to Mr. Abdul Hameed Farazi from electrical department, Mr. Saber Ali and Mr. Yones Claes Selander and other staff members from the department for their prompt and timely help.

Special thanks are due to my cousin Syed Atif Malik and friends Mujtaba bhai, Arshad, Imran, Iqbal bhai, Noman bhai, Saif, Ameen, Jalal bhai, Farooq, Sana, Farrukh, Hasan, Bilal, Ahsan, Sohail, Nayeem, Riaz, Mujahed, Jameel, Nazim, Khusro, Haseeb, Gayaz, Sami, Humayun and Qayum, who were always there to help me and provided wonderful company and some memories that will last a lifetime.

Last but not least I am grateful to my parents for their extreme moral support and continuous encouragement throughout the course of my studies at KFUPM as well as throughout my academic career. No personal development can ever take place without the proper guidance of parents.

TABLE OF CONTENTS

Page

Page

LIST OF TABLES

Page

LIST OF FIGURES

Page

THESIS ABSTRACT

Name: Syed Iftekhar Mahmood

Title: Impact testing of brittle materials using split Hopkinson pressure bar technique

Major Field: Mechanical Engineering

The high strain-rate compressive behavior of structural materials (ductile and brittle) are quite important, and can be obtained using different experimental techniques, such as falling weight or impacting mass technique, but the accuracy of measurements decreases with the increase of the strain rate. However, the split Hopkinson pressure bar apparatus (SHPB) can provide the solution since, in this case, practical test execution is relatively simple, and interpretation of the test results is relatively straightforward. It is required for a material under test in a SHPB technique to deform homogeneously and at a nearly constant strain rate; therefore this technique is limited for only ductile materials.

Brittle materials (ceramics, rocks) play a vital role in many engineering applications. Therefore, during the last decade there have been numerous developments in the conventional SHPB technique in order to obtain high strain-rate behavior of these materials. Due to certain limitations in the developed techniques, the current work aims at certain modifications in order to facilitate the dynamic testing of brittle materials along with its data analysis.

The first proposed modification relates to the replacement of the cylindrical striker bar of the classical SHPB with a spherical ball. This helps generate a smoothly increasing compressive pulse followed by an unloading tensile one, which was found recommendable in previous works to obtain high strain-rate compressive behavior of brittle materials.

The second proposed modification involves the numerical simulation of the SHPB test, aiming at calculating the reflected wave, then comparing it with the measured experimental one. This helps in obtaining the compressive failure strength of brittle materials at different strain-rates in a simple manner.

Master of Science Degree
King Fahd University of Petroleum and Minerals
Dhahran, Saudi Arabia
January 2004

ملخص الرسالة

الإسم : سيد افتخار محمود

العنوان: الإختبار التصادمي للمواد القصفة باستخدام طريقة هوبكنسون

التخصص : هندسة ميكانيكية

يعتبر سلوك المواد الإنشائية (اللدنة منها والقصيفة) في ظروف تحميل الضغط بمعدلات انفعال عالية موضوعا في غاية الأهمية . ويمكن تحديد هذا السلوك باستخدام طرق اختبار مختلفة ، مثل الأحمال المتساقطة والصدم بالكتل السريعة، ولكن هذه الطرق كلها تعاني من دقتها التي تتناقص مع زيادة سرعة التحميل . ومن ناحية أخرى ، فإن جهاز هوبكنسون للتصادم يمكن أن يحقق الحل المناسب نتيجة لسهولة إجراء الإختبار في هذه الحالـة ، وكذلك لسهولة تفسير النتائج بطريقة مباشرة . وتمتاز هذه الطريقة في حالة استخدامها مع المواد اللدنة بتحقيق انفعال منتظم في عينة الإختبار وبمعدل انفعال ثابت.

وتعتبر المواد االقصيفة من المواد التي تلعب دورا هاما في مختلف التطبيقات الهندسية . ولذلك ، تمت خلال العقد الماضي محاولات كثيرة لتطوير جهاز هوبكنسون المعتاد من أجل تحديد سلوك هذه المواد تحت معدلات انفعال عالية . ونتيجة لوجود عدة قيود في هذه المحاولات فإن البحث الحالي يهدف إلى اقتراح عدة نواحي لتطوير الجهاز من أجل تسهيل إجراء الإختبار وكذلك تحليل نتائجه.

وترتبط أول نواحي التطوير بإحلال كرة معدنية مستديرة مكان عمود التصادم في جهاز هوبكنسون- وهذا الإقتراح يساعد على تحقيق موجة اجهاد تضاغط تصادمي تتزايد فيمتها بانتظام ، يتبعها موجهة اجهاد شد تنازلية ، مما يحقق ظروف الإختبار المناسبة للمواد القصيفة كما اقترحتها الدراسات السابقة.

أما اقتراح التطوير الثاني فيتعلق بالمحاكاة العددية لاختبار هوبكنسون ، مما يحقق حساب الموجة المنعكسة من عينة الإختبار بطريقة دقيقة ، ومن ثم مقارنتها بمثيلتها المقاسة تجريبيا . وهذه الطريقة تساعد على تحديد إجهاد الإنهيار للمادة القصيفة بطريقة سهلة ومباشرة.

درجة الماجستير

جامعة الملك فهد للبترول والمعادن

الظهران ، المملكة العربية السعودية

يناير 2004م

CHAPTER 1

INTRODUCTION & BACKGROUND

1.1 Problem Statement

The number of applications in which structural elements are subjected to high strain rate loading is very widespread. These loads can be caused by accidents, such as collisions or falling objects, or can be inherent in the basic working conditions of the system (internal combustion, high frequency vibration, etc). Dynamic loads can also appear as a result of wear or bad maintenance, resulting in hammering between elements (Johnson, 1972; Verleysen, 2000)

Other examples include the case of a bird-strike on aero-engine blades, the design of shields to contain fragments from a bursting pressure vessels or high-speed rotor, impact of runway debris on aircraft composite panels (cf. Concorde accident in 2001), plastic flow close to rapidly propagating cracks and many conventional metal working or forming processes where very large strains are applied in very short times. As a consequence, dynamic experiments are essential (e.g. Follansbee, 1985; Field et al, 1998).

Because of their specific properties, brittle materials are used in almost all fields of engineering. Concrete is a well-established material in civil constructions, ceramic

parts are used in applications ranging from textile machines to bearings in combustion engine parts, thermoset plastics are used in automotive panels and telecommunications etc.

The high strain-rate behavior of ductile and brittle materials can be obtained with different experimental techniques, such as falling weight or impacting mass technique, but the quality of measurements decreases with the increase of the strain rate. The main reason is that the assumption of an instantaneous equilibrium in the loading frame and the measuring device used in these techniques, which usually neglects wave propagation effects, is not valid (Frew, 2001). Consequently, these methods of testing begin to lose accuracy at medium strain rates and special short loads cells must to be used (Harding, 1988). However, the split Hopkinson bar apparatus (SHB) can provide the solution since, in this case, practical test execution is relatively simple, and interpretation of the test results is relatively straightforward.

The SHB technique was originally designed for obtaining stress-strain data for ductile materials. Due to certain limitations for testing brittle materials, as discussed in the later sections, many investigators have introduced certain modifications in the classical SHB, but still more are required. *Therefore the present thesis aims for certain modifications in order to facilitate the dynamic testing of brittle materials along with its data analysis.*

In the following sections, the fundamentals of the SHB technique along with complications involved in testing brittle materials, proposed solutions by various researchers, objectives of the present work and finally organization of the present thesis will be presented.

1.2 Fundamentals of Split Hopkinson Bar testing

Initially, the SHB was used for compression testing (Kolsky, 1949), hence the name SHPB. Later, tension, torsion, direct shear, bending, and combined loading were introduced and developed (Field et al, 1998).

In the classical split Hopkinson pressure bar test, a short cylindrical specimen is sandwiched between two long elastic metallic bars known as input and output bars, as shown in Fig.1.1. The ends of the pressure bars and specimen are machined flat to enforce prescribed boundary conditions. A compressive stress pulse of square shape is generated at the far end of the input bar with the help of a cylindrical striker bar of specific length. This pulse travels along the bar towards the input bar-specimen interface where, because of impedance mismatch, it is partially reflected back into the input bar and partially transmitted through the specimen and into the output bar. The reflected pulse is reflected as a wave in tension, whereas the transmitted pulse remains in compression, until it reflects from the far free end of the output bar as a tensile wave.

The strain histories in the two pressure bars are recorded by strain gages at A and B. So long as the bars remain under their elastic limits, the specimen stress, strain, and strain rate may be calculated from the recorded strain histories (e.g. Wasley, 1973). The specimen stress is calculated from:

$$\sigma_s(t) = \frac{EA_o\varepsilon_T(t)}{A_s} \tag{1-1}$$

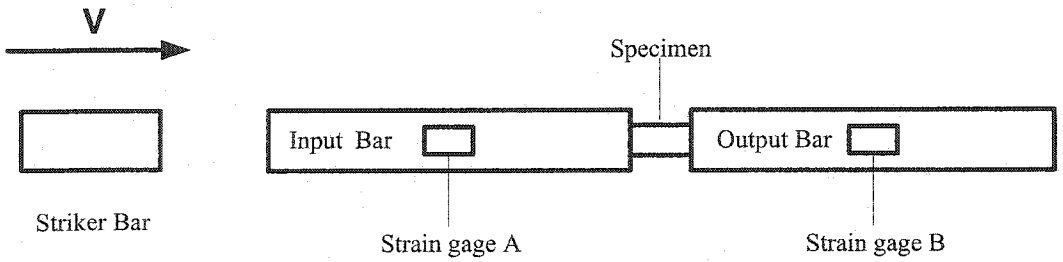

Fig. 1.1 Principle of the classical split Hopkinson pressure bar test

where E is the elastic modulus of pressure bar, A_0 and A_s are the cross sectional areas of the output bar and sample, and $\varepsilon_T(t)$ is the transmitted wave strain history.

The specimen strain rate is calculated from:

$$\dot{\varepsilon}_s = \frac{d\varepsilon_s(t)}{dt} = \frac{2C_o}{l_s}\varepsilon_R(t) \tag{1-2}$$

where $\varepsilon_R(t)$ is the reflected wave strain history, L_s is the specimen length prior to impact, and C_0 is the uniaxial wave velocity in the bar material, given by:

$$C_o = \sqrt{\frac{E}{\rho}} \tag{1-3}$$

where E and ρ are the elastic modulus and density, respectively, of the bar material. Equation (1-2) can be integrated to yield the specimen strain as:

$$\varepsilon_s(t) = \frac{2C_o}{l_s}\int_0^t \varepsilon_R(t)dt \tag{1-4}$$

Equations (1-1)-(1-4) are derived in detail in Appendix A.

There are three major assumptions in deriving the above equations, as noted by many investigators (e.g. Follansbee, 1985; Ravichandran and Subhash, 1994), namely:

a) The specimen undergoes homogeneous deformation during the experiment. This ensures that the stress within the specimen is equilibrated. This can usually be satisfied by using a specimen length such that the duration of the stress pulse employed is much greater than the transit time for the stress pulse in the specimen.

b) The various stress pulses (incident, reflected and transmitted) encountered in the split Hopkinson bar undergo minimal dispersion. This assumption ensures that the signals recorded from strain gages, which are placed on the input, and output bars are true

measures of the response of the specimen. This also implies that the variations of stresses and displacements over the cross section of the bar are negligible, i.e., one-dimensional state prevails. This has important implications in studying the high strain rate response of brittle materials, especially when the specimens fail in a very short duration (a few microseconds).

c) The bars remain elastic at all times, and their ends in contact with specimen remain flat and parallel throughout the experiment. Making the input and output bars of high-strength material usually meet this assumption.

This technique had been used to measure the dynamic compressive properties of almost all ductile materials. A comprehensive review has been reported by Eleiche (1972).

1.3 Complications in Testing Brittle Materials

The following criticisms can be made regarding the classical SHPB technique.

i. The SHPB is mainly used to investigate the dynamic flow behavior of *ductile* metal. Hence, the results at small strains are not considered valid owing to fluctuations associated with the early portion of the reflected signal and the non-equilibrated stress state in the specimen. When elastic and small-strain behavior is important, such as in the case of brittle materials, the accuracy of the conventional SHPB is not acceptable.

ii. The technique also requires the sample to deform under constant strain rate. In the classical Hopkinson bar technique, this is accomplished by seeking to impart a constant stress pulse into the incident bar. But the constant stress pulse does not produce a constant strain rate. Instead, it deform the sample in three distinct regimes, namely, an initial regime of positive strain rate, when the stress in the sample

increases to a constant level, followed by a regime of zero strain-rate, which is then followed by a regime of negative strain rate (Nemat-Nasser, Issacs and Starrett, 1991).

Some results reported in the literature showing the effect of strain rate on some brittle materials are given in Figs. 1.2 and 1.3 for PMMA and in Figs. 1.4 and 1.5 for Concrete. The experimental techniques used were different than those used in the classical SHPB.

1.4 Proposed Solutions

To overcome the problems mentioned in the previous section, many investigators have developed novel techniques for the SHPB experiments, in which they recommended pulse shaping in order to achieve a ramp pulse in the incident bar. The investigators emphasized that a slowly rising incident pulse is preferred to a pulse that rises steeply in order to minimize the effects of dispersion and allow the sample to achieve dynamic stress equilibrium along with the constant strain rate.

Such novel techniques developed for dynamic compression tests along with experimental results obtained on a typical brittle material (SiC) are discussed in Chapter2.

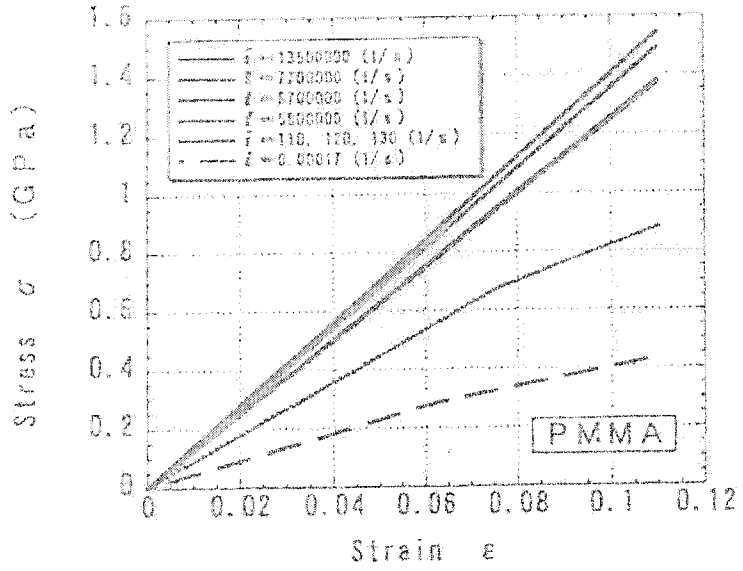

Fig. 1.2 Stress-strain curves at various strain rates for PMMA under conditions of uniaxial strain using plate impact experiments (Sato and Kituchi, 2001)

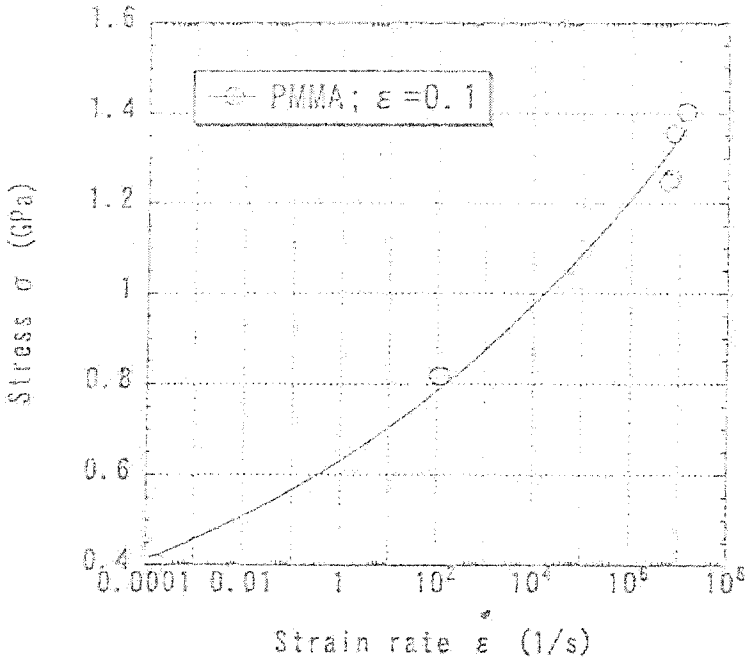

Fig. 1.3 Stress as a function of strain-rate for PMMA under conditions of uniaxial strain using plate impact experiments (Sato and Kituchi, 2001)

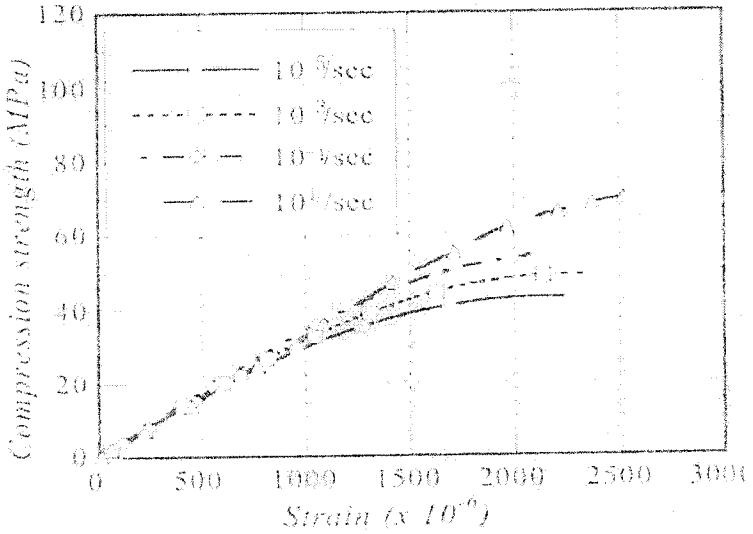

Fig. 1.4 Effect of strain-rate on stress-strain curve for concrete (Shirai, Yagishita and Ito, 2001)

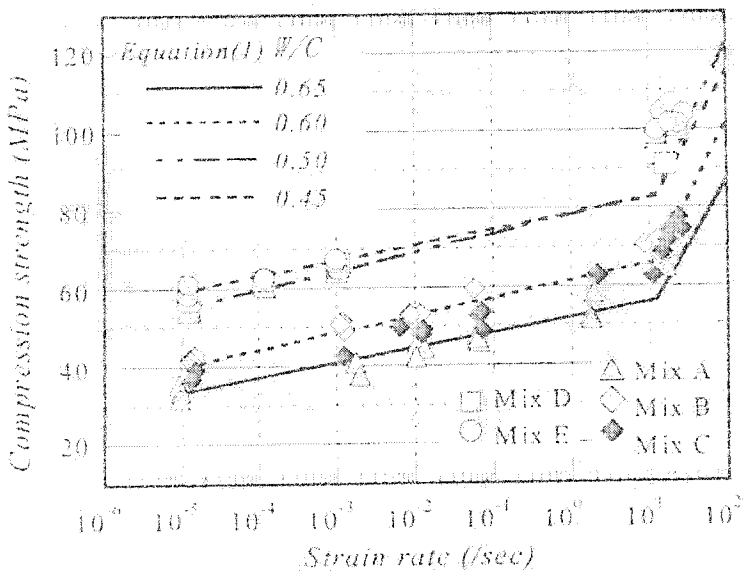

Fig. 1.5 Effect of strain-rate on dynamic compressive strength of concrete (Shirai, Yagishita and Ito, 2001)

1.5 Objectives of the Present Work

The main objectives of the current thesis are:

i. To propose a new simple method to produce ramp compressive loading followed by unloading, through theoretical analysis and confirmation by experiment. The method is detailed in Chapter3.

ii. To propose and apply a new approach to obtain the material strength at different constant strain rates by numerically simulating the experiment and comparing calculated pulses with the measured ones. Details are presented in Chapter4.

1.6 Thesis Organization

Chapter 2 provides a critical review of previous work, and a proposed methodology for testing brittle materials. Chapter 3 presents the proposed method to introduce an incident ramp loading in the SHPB test. Chapter 4 discusses the proposed numerical simulation of the experiment. Finally, Chapter 5 presents the conclusions and some recommendations for future work.

CHAPTER 2

REVIEW OF PREVIOUS WORK

2.1 Introduction

The split Hopkinson pressure bar (SHPB) technique, originally developed by Kolsky (1949), has been used by many investigators to obtain dynamic compression properties of solids. The evolution of this experimental method and recent advances are discussed by Nicholas (1982), Ellwood, Griffiths and Parry (1982), Follansbee (1985), Nemat-Nasser, Isaacs and Starrett (1991), Field et al (1998), Frew, Forrestal and Chen (2001). This technique is mostly used to study the plastic flow stress of materials that undergo large strains at strain rates between 10^2-10^4 s^{-1}. It is usually agreed that collected data are typically obtained for strains larger than a few percent because the technique is not capable of measuring the elastic and early yield behavior (Nemat-Nasser, Isaacs and Starrett 1991).

In contrast, most of the advanced materials of interest such as ceramic composites (which possess exceptional mechanical properties) are relatively brittle and reach their full strength at strains less than about 1.0 percent. The determination of the dynamic compressive strength of these materials poses a challenging problem because in an ideal Kolsky compression bar experiment, the sample should be in dynamic stress equilibrium

and deform at a nearly constant strain rate over most of the test duration. For the stress-strain response of relatively brittle materials that have a nearly linear response to failure, the classical SHPB needs certain modifications. In order to overcome this problem many researchers recommended the shaping of the incident as discussed below.

Christensen, Swanson and Brown (1972) used striker bars with a truncated-cone on the impact end in an attempt to produce ramp pulses. Franz, Follansbee and Wright (1984) discussed experimental techniques for pulse shaping and a numerical procedure for correcting raw data for wave dispersion in the bars. In a comprehensive review paper, Follansbee (1985) discussed pulse shaping using metal samples for SHPB experiments. He had also emphasized that a slowly rising incident pulse is preferred to a pulse that rises steeply in order to minimize the effects of dispersion and allow the sample to achieve dynamic stress equilibrium. Nemat-Nasser, Isaacs and Starrett introduced in 1991 a novel technique to adapt the classical SHPB for testing of brittle materials. They introduced pulse shaping with properly designed OFHC disk to achieve a ramp pulse in the incident bar, while measuring the specimen strain by attaching strain gauges directly on its surface. Later on, Togami, Baker and Forrestal (1996) used a thin Plexiglas disk to produce non-dispersive compression pulses in the incident bar. Frew, Forrestal and Chen (2001) also presented pulse shaping techniques, whereby thin disks of annealed or hard C11000 copper were placed on the impact surface of the incident bar in order to shape the impacting pulse.

In the following sections the novel techniques developed by Nemat-Nasser, Isaacs and Starrett (1991) and Frew, Forrestal and Chen (2001) are presented. Some results

obtained for the behavior of typical materials are also shown. The major drawbacks of the methods used are finally discussed and a proposed solution presented.

2.2 Modifications of Split Hopkinson Pressure Bar

2.2.1 By Nemat-Nasser, Isaacs and Starrett (1991)

The experimental technique used two changes in the conventional split Hopkinson pressure bar (Fig.2.1):

a) A thin metal cushion is placed at the end A of the incident bar

b) The specimen strain is measured directly by attaching strain gauges to its surface.

The presence of the cushion introduces a monotonically increasing ramp-like stress pulse in the incident bar. The average strain at which the test can be performed, is limited in this technique. Since the strain is measured directly on the specimen as a function of time, reliable information is obtained. The measured incident and transmitted pulses, gives the complete axial stress history of the sample, while the axial and lateral strain histories are measured by two strain gauges on two adjacent lateral faces of the sample.

It can be seen from Eq. (1-2) used to determine the strain rate in the classical split Hopkinson pressure bar experiment, it is necessary that $\varepsilon_r = -(\varepsilon_I - \varepsilon_t)$ be constant in order to make the sample strain rate constant. This is achieved by seeking to impart a stress pulse, having a very short rise time and constant amplitude thereafter, into the incident bar. However, in an elastic sample a constant stress pulse cannot produce constant strain rate; instead, it deforms the sample in three distinct regimes, namely, initial regime of positive strain rate, when the stress in the sample increases to a constant

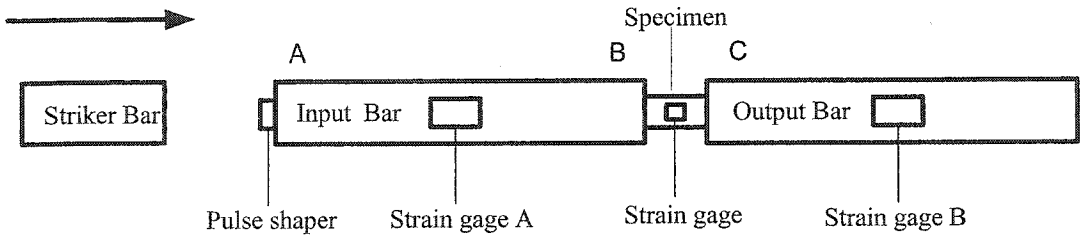

Fig. 2.1 Modification of SHPB (Nemat-Nasser, Issacs and Starrett, 1991)

level, followed by a regime of zero strain rate, which is then followed by a regime of negative strain rate.

Thus in the novel technique adopted, the strain rate (ε_I-ε_T) is tried to be kept nearly constant as possible by using a ramp pulse produced by the deformation of a metal cushion. This metal cushion, also called the pulse-shaper, is made of a properly selected material and to critical dimensions, introduces a monotonically increasing ramp-like stress pulse in the incident bar as shown in Fig.2.2. Since the sample response is linear, essentially up to the failure stress, the ramp-like pulse is ideal to subject the sample to a constant strain rate up to fracture.

Moreover, the specimen strain rate is usually measured from the deformation-time history of the specimen, as seen in Fig.2.3. This is discussed in some detail in the next section.

2.2.2 By Frew, Forrestal and Chen (2001)

The conventional SHPB apparatus is modified also by shaping the incident pulse such that the samples are in dynamic equilibrium and have nearly constant strain rate over most of the test duration. A thin disk of annealed or hard C11000 copper is placed on the impact surface of the incident bar as shown in Fig.2.4. After impact, the pulse shaper deforms plastically and spreads the pulse in the icindent bar. In their work, the authors also present an analytical model and experimental data that show a wide variety of incident strain pulses produced by varying the geometry of the pulse shapers and the length and striking velocity of the striker bar. Figs. 2.5 & 2.6 represents the experimental data and model predictions for incident stresses from pulse shaped experiments using hard (HRB 45) and annealed C11000 pulse shapers.

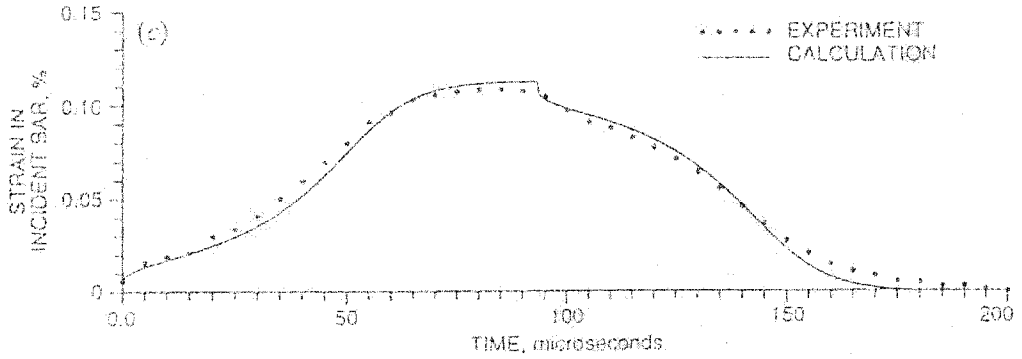

Fig. 2.2 Strain profile generated by a 9 inch striker bar at 11.02 m/s velocity with an OFHC cushion of 0.190 inch initial diameter and 0.020 inch thickness (Nemat-Nasser, Issacs and Starrett, 1991)

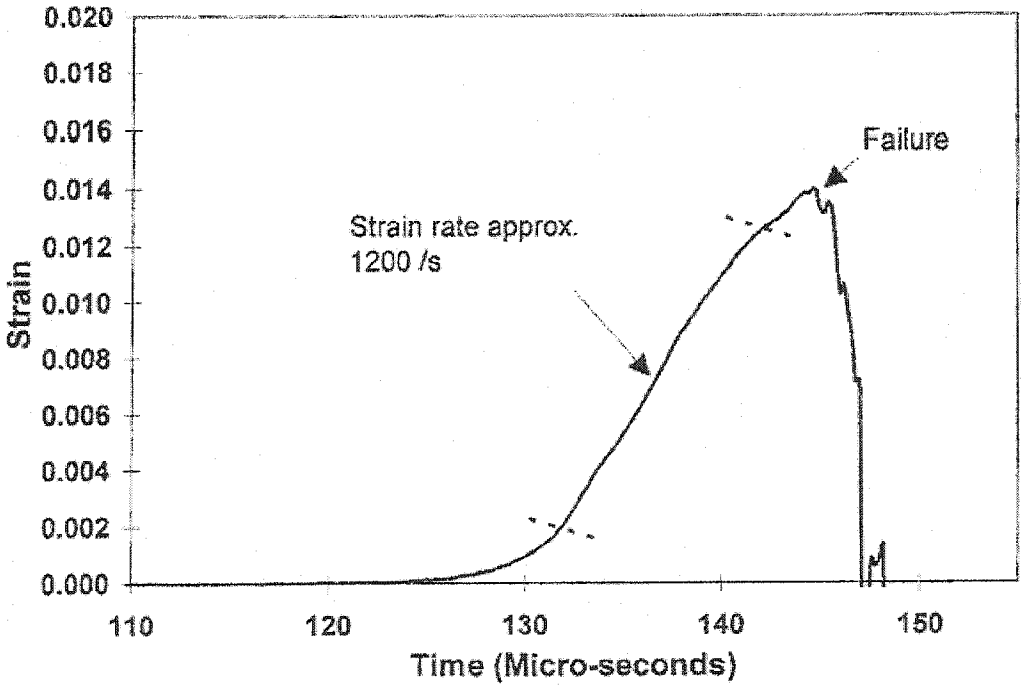

Fig. 2.3 Deformation-time history of the specimen (Sarva and Nemat-Nasser, 2001)

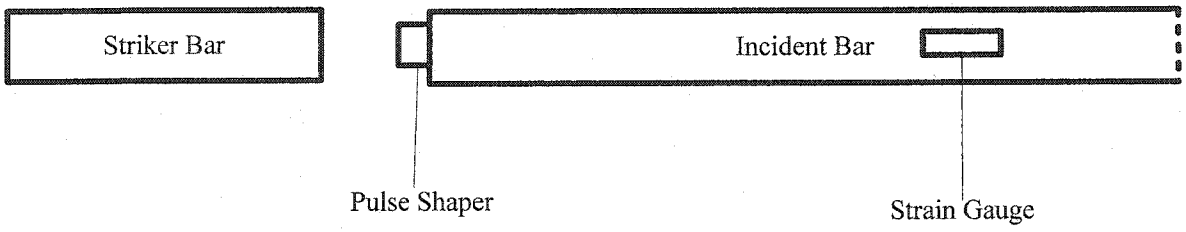

Fig. 2.4 Schematic of the loading end of a SHPB with a pulse shaper (Frew, Forrestal and Chen, 2001)

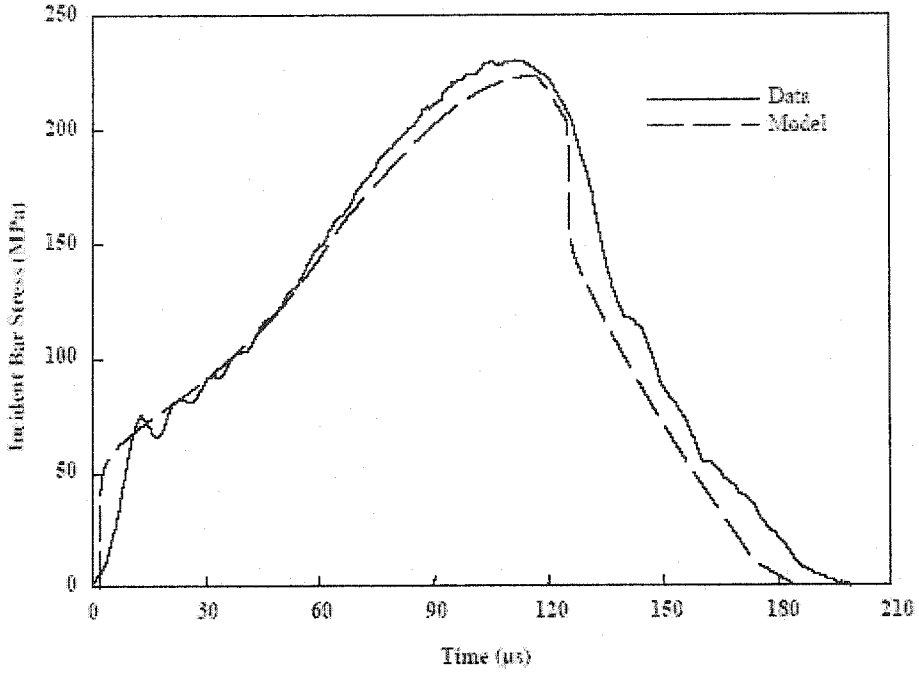

Fig. 2.5 Incident bar stress data and model prediction for a hard C11000 copper pulse shaper (Frew, Forrestal and Chen, 2001)

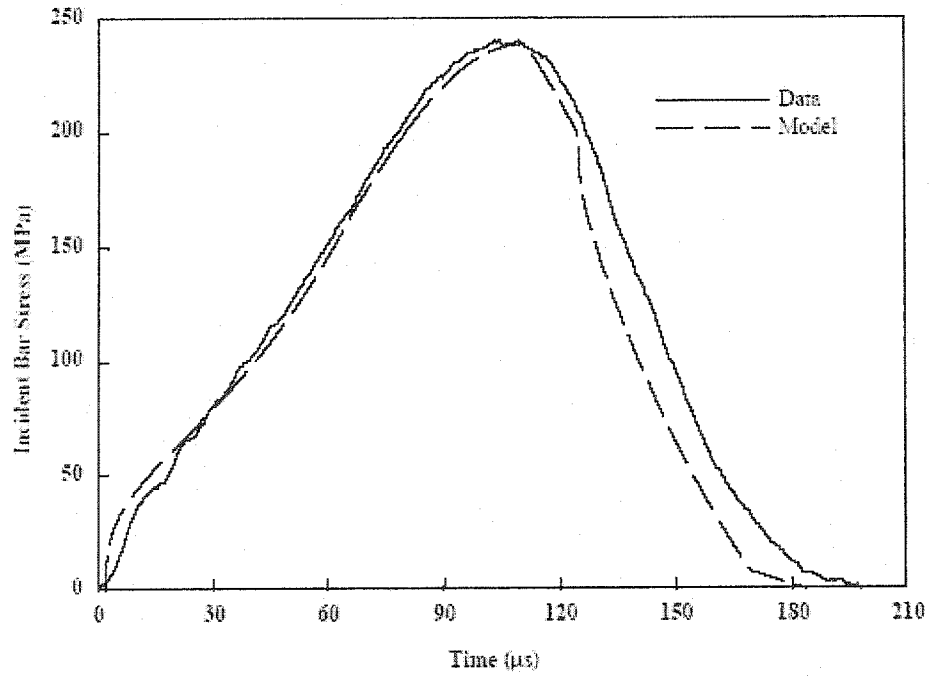

Fig. 2.6 Incident bar stress data and model prediction for an annealed C11000 copper pulse shaper (Frew, Forrestal and Chen, 2001)

2.3 Experimental Results Obtained by Sarva and Nemat-Nasser Using a Modified SHPB (2001)

Sarva and Nemat-Nasser used a SHPB modified as explained above to test Silicon Carbide. Figure 2.7 shows the time resolved voltage output from strain gauges attached on the input and output bars of a sample test. The failure strength is calculated from the transmitted pulse, using Eq. (1-1).

Since the failure strains in SiC are very low, the resulting reflected pulse is thus very weak and cannot be taken as an accurate measure of the strain in the sample. Therefore, the sample strain was measured from strain gauges fixed directly on the specimen. Figure 2.8 is the strain-time profile calculated from the output of the strain gauge attached axially on the sample. The sample is loaded for approximately 20 μs, prior to failure. As can be seen, the sample strain rate achieved is constant at about 1200/s. Figures 2.7 and 2.8 are important ones for this thesis, and will be discussed in great detail in Chapter 4.

The stress-strain curves obtained indicated a nearly linear response up to failure, for both static and dynamic tests, indicating very little plasticity. The effect of strain rate on the compressive failure strength of SiC is seen in Fig. 2.9. The compressive strength under quasi-static testing conditions is approximately 4.2 GPa. Dynamic tests confirm the strain rate sensitivity of this material. The strength increases to 4.2 GPa at a strain rate of 250/s, and further to 7.0 GPa at 1200/s.

Sarva and Nemat-Nasser also reported that the sample failed by axial splitting under both static and dynamic conditions. At peak stress, the samples shattered to

fragments. Figure 2.10 compares the fragment size for static and dynamic tests. The fragment size for the static test can be seen visibly larger than that for a dynamic test.

2.4 Criticism of Methods Used in Previous Work

There are certain limitations in the techniques discussed above for testing brittle materials, namely:

(a) In order to introduce monotonically increasing ramp-like stress pulse in the incident bar, the thin metal cushion placed at the impact end of the incident bar, should be properly designed in terms of material selection and dimensions. This is a complex and unreliable technique of pulse shaping, since a slight variation can produce an unexpected shape of the incident pulse (cf. Figs 2.2, 2.5 and 2.6)

(b) Since the resulting reflected pulse is not an accurate measure of the strain in the sample, Sarva and Nemat-Nasser obtained the axial strain history by attaching strain gauges directly on the specimen surface. Fixing strain gauges on the specimen is not always a practical approach especially if the specimen size is too small which reflects on the accuracy and cost involved. Moreover, the approach dictates scarifying the strain gauge and wiring with each test, which implies unaffordable costs, particular when a large scatter in the results is involved.

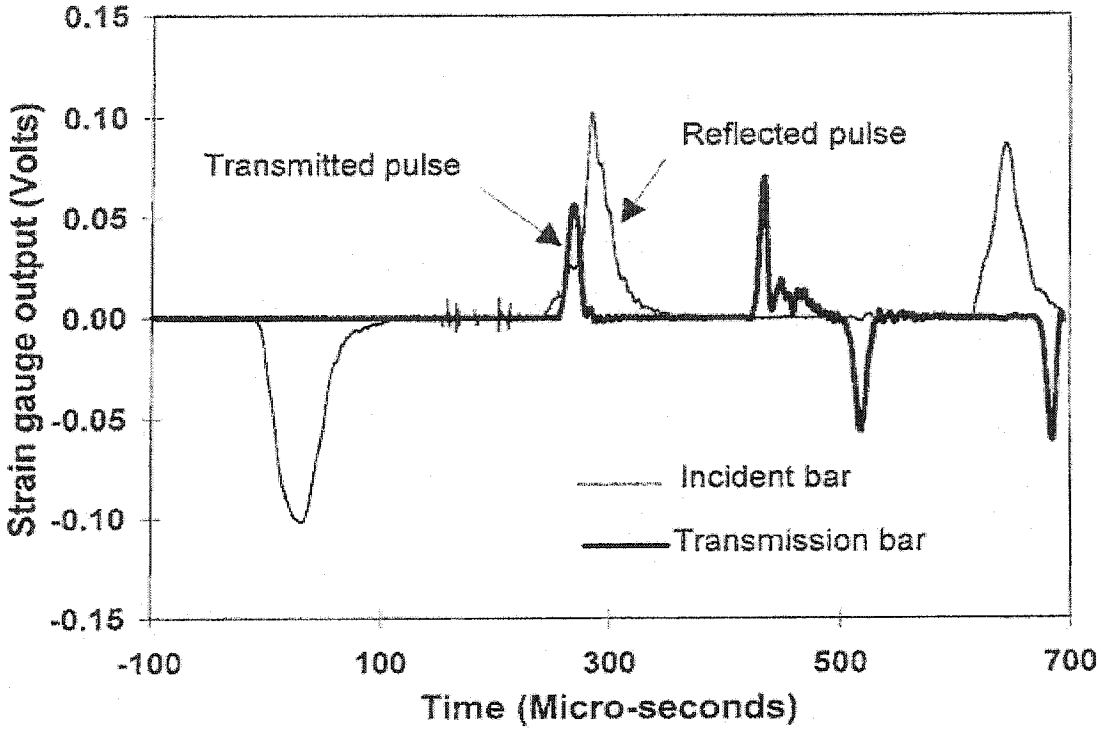

Fig. 2.7 Output obtained from strain gauges on I/P and O/P bars (Sarva and Nemat-Nasser, 2001)

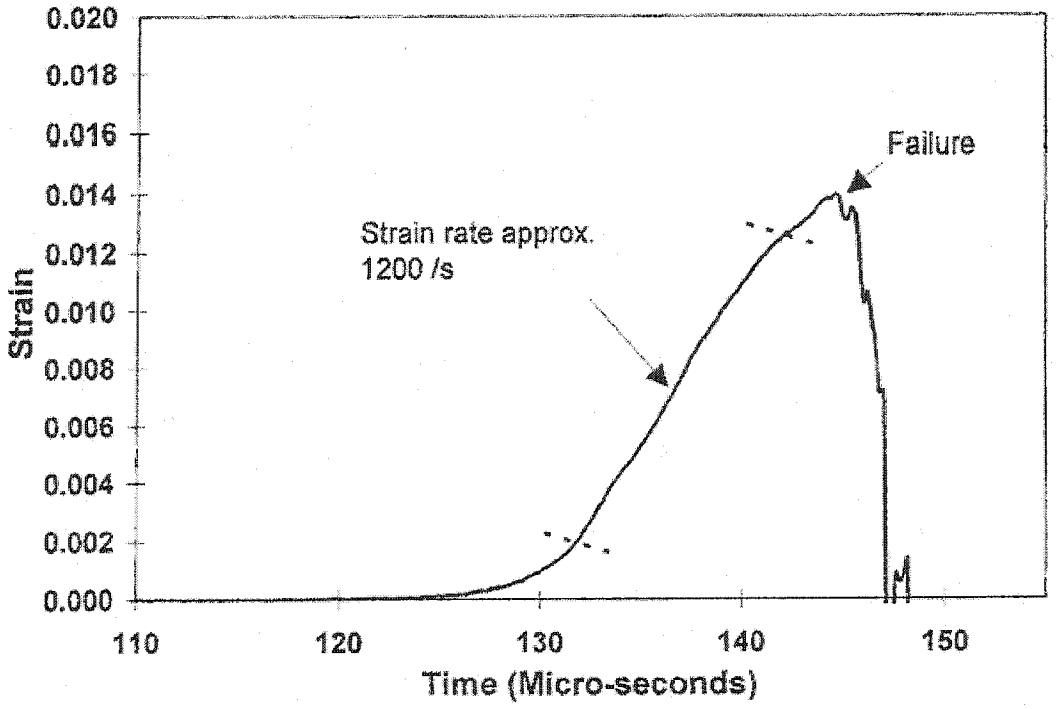

Fig. 2.8 Strain profile obtained from strain gauges on the sample (Sarva and Nemat-Nasser, 2001)

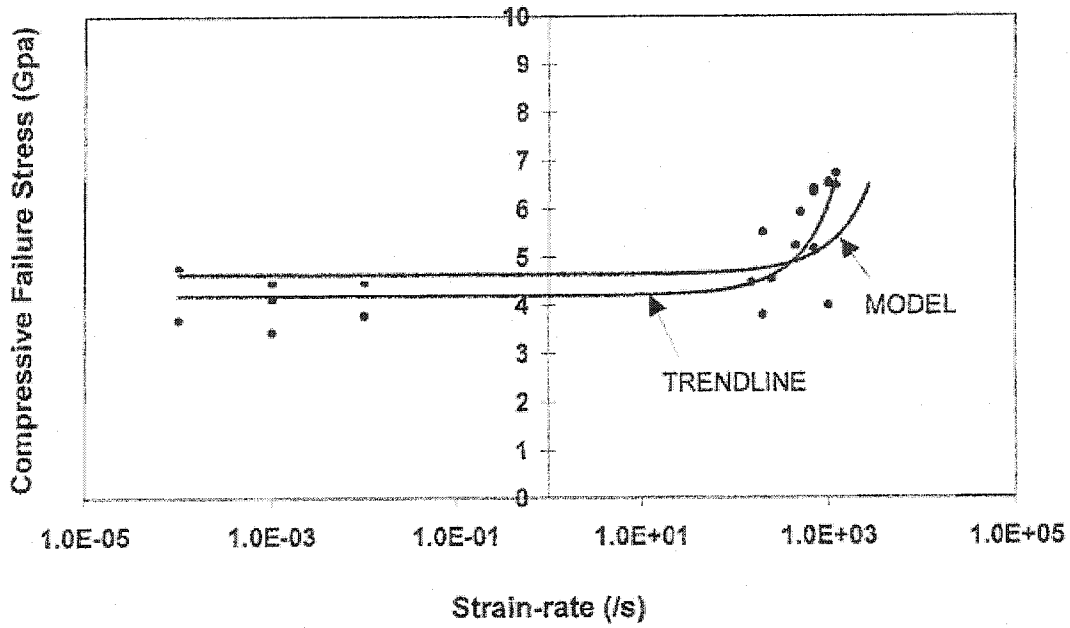

Fig. 2.9 Experimental results for compressive failure strength
(Sarva and Nemat-Nasser, 2001)

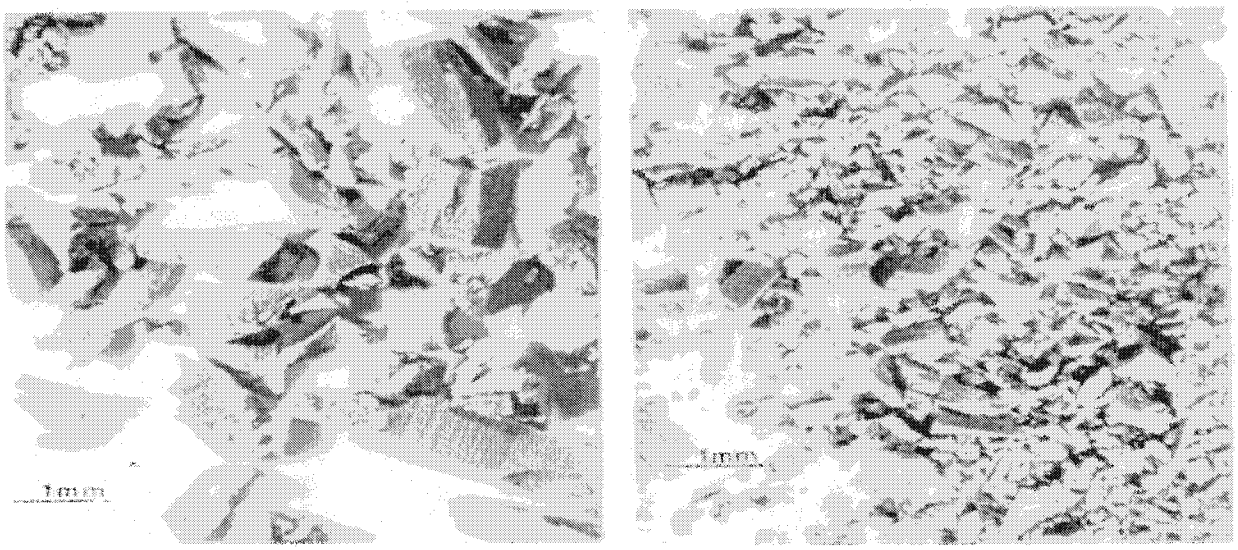

Fig. 2.10 Comparison of fragment size for static and dynamic tests
(Sarva and Nemat-Nasser, 2001)

2.5 Proposed Solutions in the Current Thesis Work

In order to rectify the above-mentioned problems involved in the previous work reported on brittle materials other solutions are proposed in the present thesis. These are briefly described in the following.

2.5.1 Proposed methodology for producing a ramp loading

In this method, the cylindrical striker bar of the classical SHPB is replaced by a spherical ball. This helps generate a smoothly increasing compressive pulse followed by an unloading tensile one. To prevent indentation of the input bar, its surface should be properly hardened. The theoretical analysis of this situation involving different diameter spherical balls hitting a long cylindrical bar of given diameter had been performed. The results are presented in the next chapter and also compared with experimental traces.

2.5.2 Proposed methodology for the analysis of the experimental data

A numerical study involving the simulation of the test is proposed, aiming at calculating the reflected wave, then comparing it with the measured one. The procedure involves estimating beforehand the amplitude of the specimen strength at the strain rate of the test. A few iterations usually yield the proper value. Details of this method and its application are given in Chapter 4.

CHAPTER 3

PROPOSED METHOD FOR GENERATING AN INCIDENT RAMP LOAD

3.1 Introduction

As discussed in the previous chapters, many researchers modified the conventional SHPB using the pulse-shaping technique. From this technique the dynamic properties of materials, which behave elastically, can be obtained with reasonable accuracy.

Due to the limitations discussed in Chapter 2 for pulse shaping techniques, a novel method of loading is proposed in which a cylindrical striker bar is replaced by a spherical ball. The resulting impact wave is a smoothly increasing compressive pulse followed by an unloading tensile one. For this particular impact situation, a theoretical analysis of different diameter spherical balls hitting a long cylindrical bar of given diameter is performed, and the results are presented in the following section. Based on this modification, an experimental SHPB setup is developed, manufactured, and instrumented.

3.2 Theoretical Analysis

Barton, Volterra and Citron (1958), performed a theoretical analysis for the case of a longitudinal elastic impact of a sphere on an infinitely long cylindrical bar (Fig.3.1). They also compared the analysis with experimental results for different diameter of spheres.

The governing non-linear ordinary differential equation for impact of a sphere against a rod is derived in Appendix B. It is given by:

$$\frac{d^2\beta}{dt^2} + \frac{K}{\rho C_0 A}\frac{d\beta^{3/2}}{dt} + \frac{K}{m}\beta^{3/2} = 0 \qquad (3\text{-}1)$$

where β is the relative displacement of the centers of mass of ball and bar, ρ is the density, A is the cross-sectional area of the bar, E is the modulus of elasticity, υ is Poisson's ratio of the bar, C_0 is the wave velocity, which equals $\sqrt{\frac{E}{\rho}}$, m is the mass of the ball, and K is a constant dependent on the elastic and geometric properties of the contact surfaces. For the case of a spherical ball of radius r hitting a flat surface of the same material as the sphere, the formula for K is given by:

$$K = \frac{2}{3}\left[\frac{E}{1-\upsilon^2} r^{1/2}\right] \qquad (3\text{-}2)$$

where r is the radius of the ball. The derivation and solution of Eq. (3-1) are given in detail in Appendix B.

The relationship between the contact force and local deformation is determined from classical Hertz contact theory, usually given by:

$$F(t) = -K\beta(t)^{\frac{3}{2}} \tag{3-3}$$

Therefore, the stress at the impact end of the longitudinal bar is calculated by:

$$\sigma(t) = \frac{F(t)}{A} \tag{3-4}$$

where $F(t)$ is the force between the ball and the bar, A is the cross-sectional area of the cylindrical bar.

Previous equations have been programmed using Mathematica. The solution for the stress-time variation at the impact end was obtained for two cases of interest, namely:

Case (1) The conditions used by Barton, Volterra and Citron (1958) consisting of steel balls of diameters 1 and 2 inches hitting a cylindrical bar of 1inch (2.54cm) diameter at different velocities. Stress-time histories of these configurations are shown in Figs. 3.2 and 3.3, and compare identically with those given by Barton, Volterra and Citron (1958). This helps verify the calculation procedure using Mathematica.

Case (2) The conditions pertaining to the current experimental setup, consisting of a steel ball of diameter 1.7-inch diameter hitting a cylindrical bar of 0.63 inch (1.6 cm) diameter. A parametric study is performed to indicate the effect of impact velocity. The resulting stress-time histories for this configuration are shown in Fig.3.4.

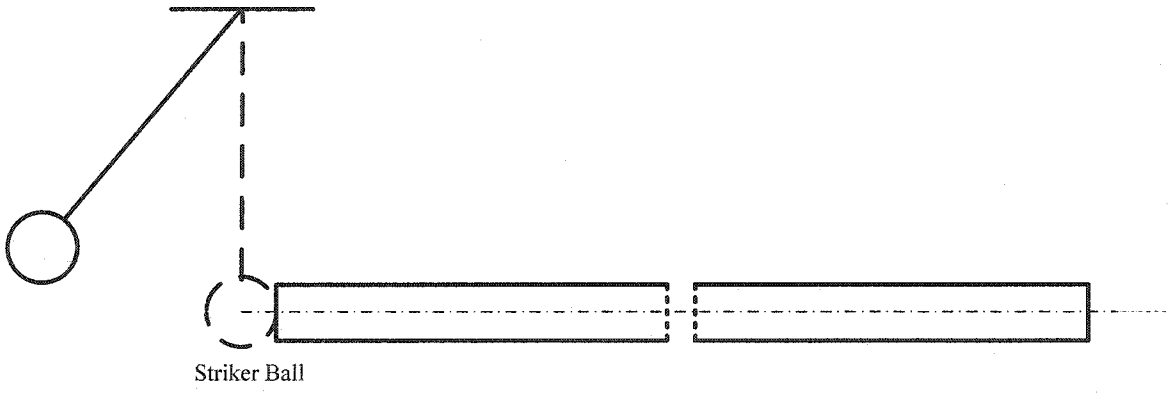

Fig. 3.1 Schematic diagram of spherical ball hitting a long cylindrical bar

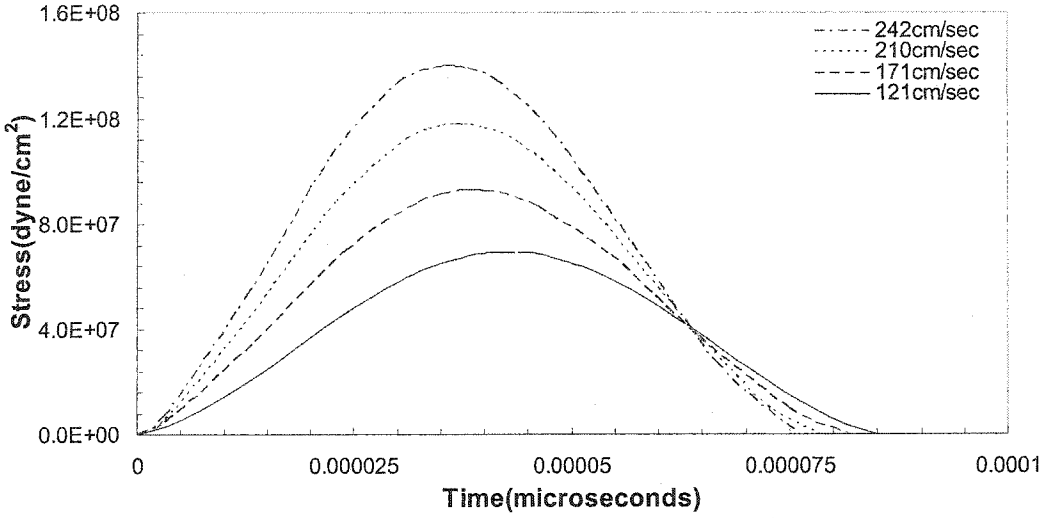

Fig.3. 2 Stress versus time at the impact end of a 1 in. dia. bar impacted by a 1in. dia. ball at different impact velocities (Barton, Volterra and Citron, 1958)

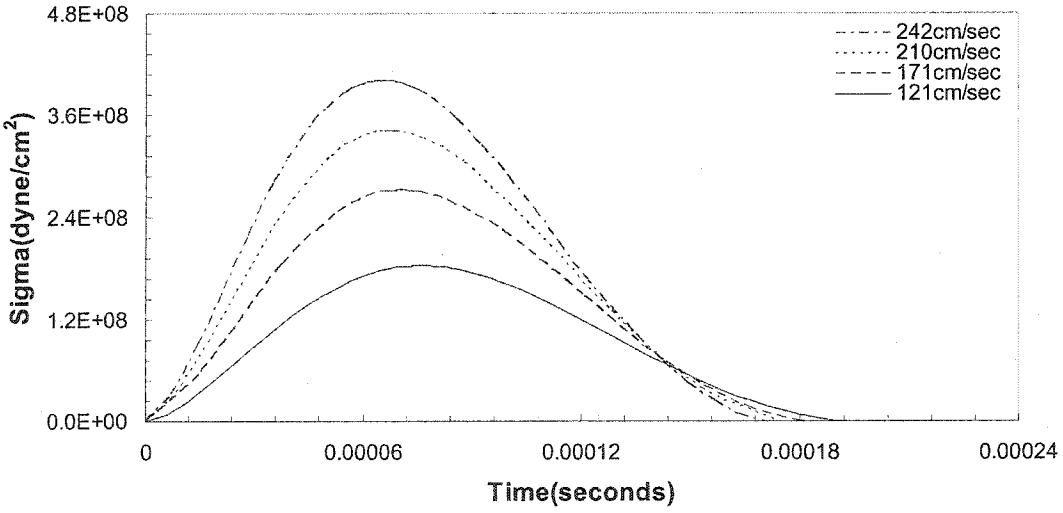

Fig.3. 3 Stress versus time at the impact end of a 1 in. dia. bar impacted by a 2 in. dia. ball at different impact velocities (Barton, Volterra and Citron, 1958)

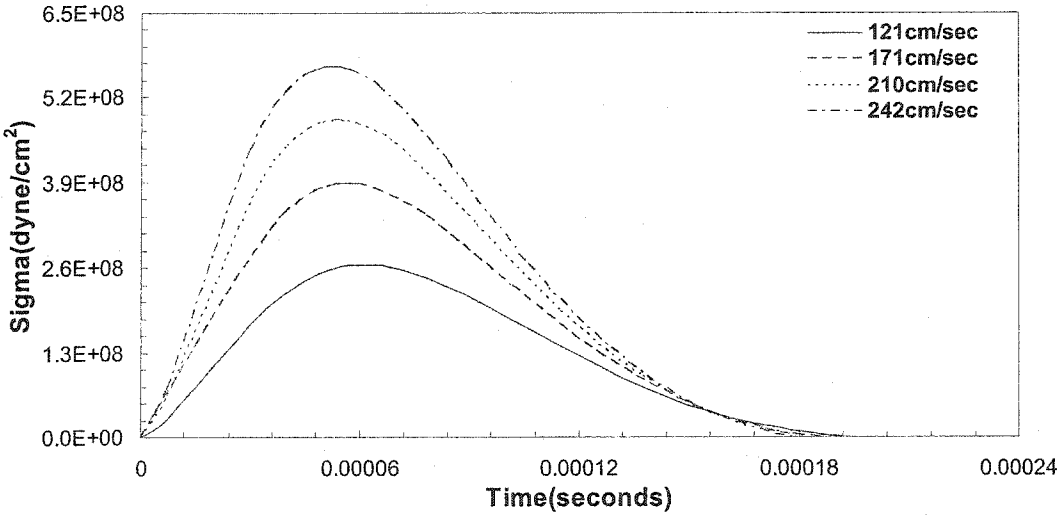

Fig.3. 4 Stress versus time at the impact end of a 0.63 in. dia. bar impacted by a 1.7 in. dia. ball at different impact velocities (current setup)

The results shown in Figs. 3.2-3.4 indicate that the maximum stress intensity achieved and the corresponding rise times obtained in the long cylindrical bar depend on the following factors.

b) The velocity at impact (corresponding to the drop height of sphere)

b) The diameter of the impacting sphere

b) The diameter of the cylindrical bar

3.3 Implementation in SHPB Setup

The basic components of the experimental setup are the same as in the classical SHPB, except for the loading arrangement. The setup is shown diagrammatically in its basic configuration in Fig. 3.5. Appendix C presents drawings and close-up photographs of the setup and its various components. The setup consists essentially of:

(a) Frame (b) Rotating Arm

(c) Impacting steel ball & housing (d) Supports

(e) Uniform steel input and output bars (f) Strain gages

The following considerations are accounted for in the designing of the setup.

3.3.1 Pressure bars characteristics

a) The yield strength of the pressure bars determines the maximum stress attainable within the deforming specimen. The two bars are made of high strength steel in the present case.

b) The length of the pressure bars is determined by conditions required for one-dimensional wave propagation, which requires approximately 10 bar diameters.

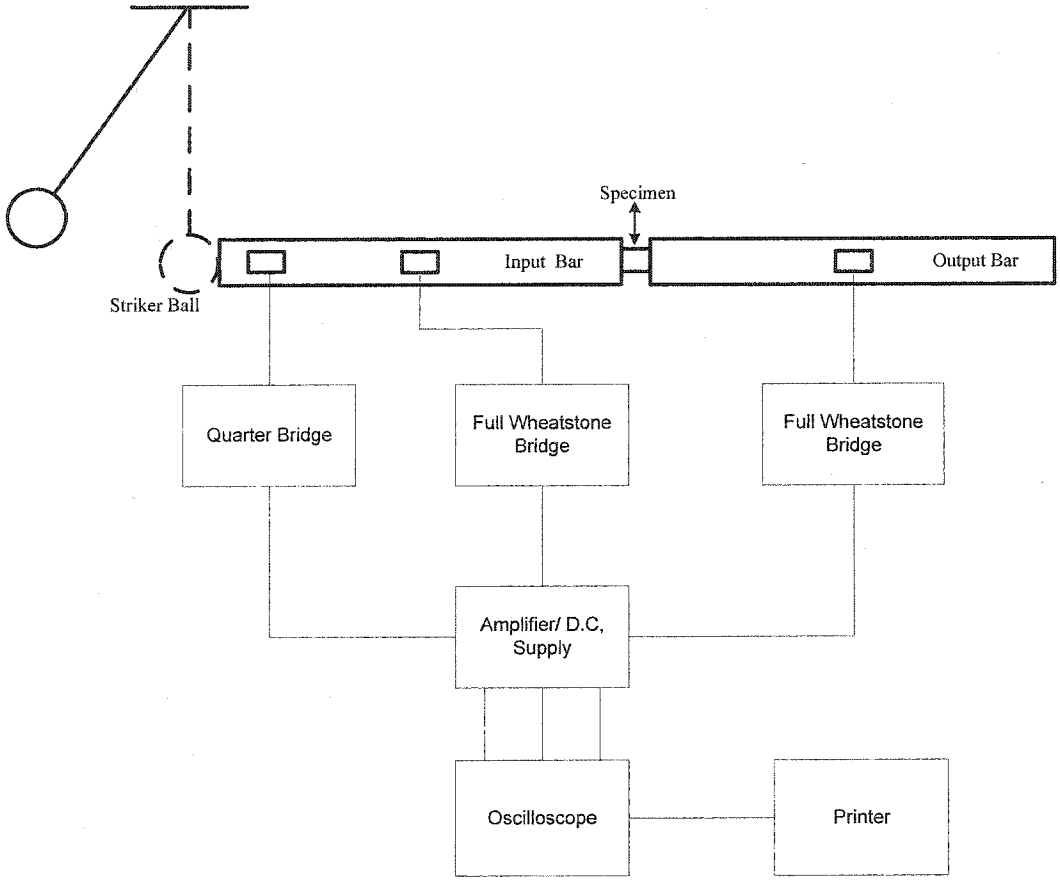

Fig. 3.5 SHPB and instrumentation

3.3.2 Bar alignment

Accurate bar alignment is required for ideal one-dimensional wave propagation within the pressure bars and for uniaxial compression within the specimen. However, alignment cannot be forced by over constraining the pressure bars, because this violates the boundary conditions for one-dimensional wave propagation in an infinite cylindrical solid. This is one reason for a tight specification on curvature in the pressure bars.

In the present setup, each bar is mounted on two wooden supports covered with Teflon, which are placed at equal distance of 40cms.

3.3.3 Mode of generating the incident wave

As explained above, a steel spherical ball is employed. The ball is attached to the end of a pendulum arm in a special holder or cage. Upon hitting the input bar, a smoothly rising compressive pulse, followed by an unloading one is generated. For an input bar of 1.6 cm diameter, and a ball diameter of 4.2 cm, the impacting wave is expected to be a s shown before in Fig. 3.4.

3.4 Instrumentation

Electrical resistance strain gauges are attached to the input and output bars to monitor the traveling wave signals. At each station, four gages are used and connected to form a 4-arm Wheatstone bridge (Fig. 3.6). The strain gages on the input bar sense the incident and reflected waves, whereas those on the output bar sense the transmitted wave.

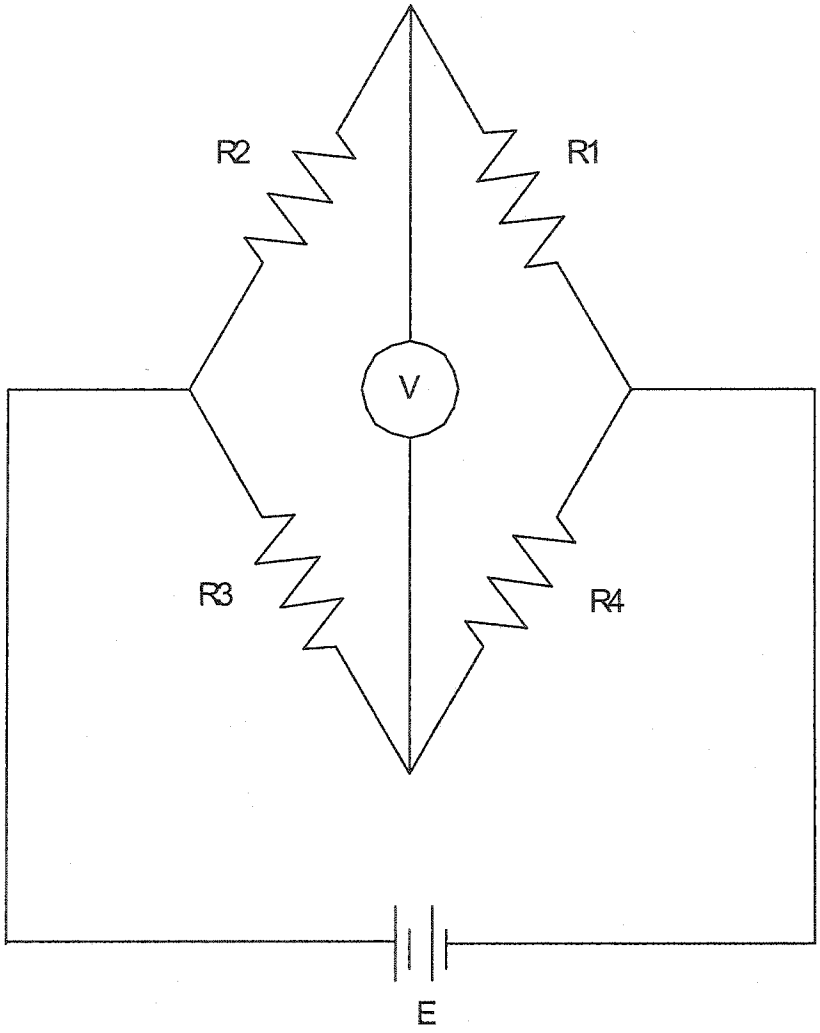

Fig. 3.6 Full Wheatstone bridge circuit

3.5 Data Acquisition

The lead wires from the strain gauges on each bar were connected to a signal conditioner on multi channel amplifier. Three channels of the amplifier were used, two for the strain-gage bridges on the input and output bars, and one for the triggering gages attached close to the impacted end of the input bar in a quarter bridge configuration.

The outputs from two amplifiers are fed to a two channels on Digital Storage Oscilloscope through BNC cables. Thus the incident, reflected and transmitted waves could be captured, and stored if required for later printing and/or analysis.

3.6 Implementation of the Developed Method of Ramp Loading to SHPB Testing

Figures 3.7 and 3.8 presents the theoretical and experimental traces for a 1.7 inch diameter ball hitting a long cylindrical bar of diameter 0.63 inch at a velocity of 1m/s. In both cases, a smoothly increasing pulse of 70 μs rise time is followed by a decreasing (unloading) pulse. The shape of the pulse in both cases is also identical.

The incident pulse took approximately 200 μs to travel from the impact end of the input bar to the other end; which is equal to the time obtained theoretically for a wave traveling at a speed of 5000 per second (speed of wave in steel) for a distance of 1 meter. The experimental traces also show the multiple reflections from the free end of the incident bar which is opposite in behavior as compared to the initial loading wave.

The amplitude of the wave depends on the mass of the impacting sphere, and its velocity at impact. The maximum energy associated with the current configuration was calculated to be 2.4 Joules at impact. This energy can only cause weak brittle materials to

fracture. For strong brittle materials, a much higher velocity should be used, which can only be obtained by using a gas gun, or similar equipment.

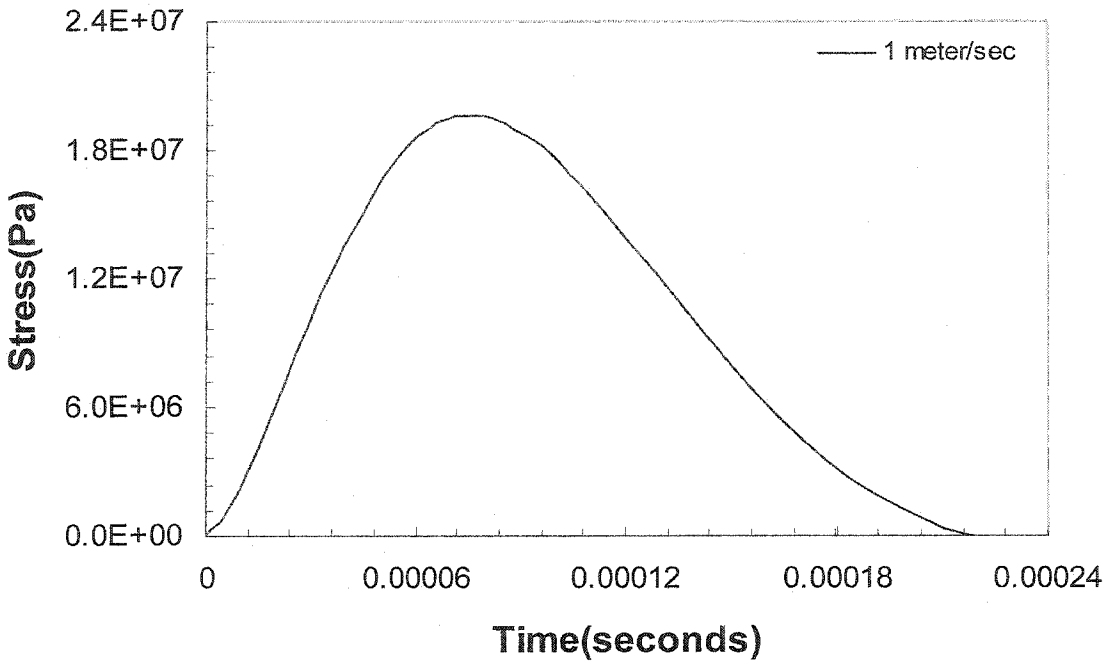

Fig. 3.7 Calculated stress history at the impact end of 0.63in. dia. bar versus time for 1.7 in. dia. ball at a velocity of 1m/s (current geometry)

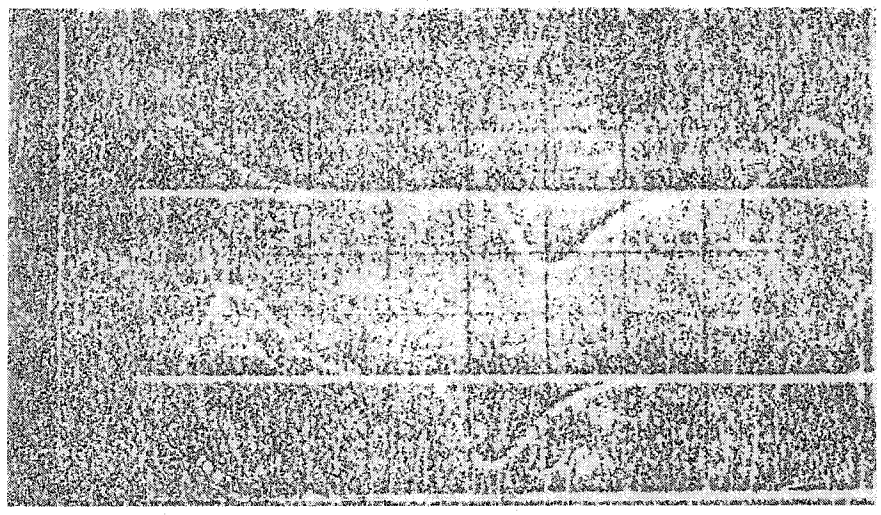

Fig. 3.8 Experimental traces obtained from the oscilloscope

CHAPTER 4

PROPOSED METHOD FOR ANALYSIS OF EXPERIMENTAL DATA

4.1 Introduction

As noted in Chapter 2, it is usually difficult to uncover the dynamic behavior of a brittle specimen experimentally, since the reflected wave is not representative of specimen behavior. In fact, it is a composite indication of many separate behaviors, namely

1. The reflection of the initial loading wave from the input bar-specimen interface up to specimen fracture.
2. The release wave from the specimen, which initiates after its fracture (Kolsky, 1973).
3. The reflection of the remaining part of the loading, after specimen fracture, from the "now" free end of the input bar.

As such, the reflected wave cannot be used to calculate the specimen strain rate, and hence strain, using Eqs. 1-2 and 1-4 as with the case of ductile materials. Therefore, a new methodology involving numerical simulation has been proposed in the Chapter 2, and will be developed and implemented in the current chapter. The proposed method is then verified by considering the experimental results presented by Sarva and Nemat-Nasser on SiC (2001), shown before in Fig. 2.7.

4.2 Numerical Simulation of Test

The numerical simulation of the SHPB test is based on assuming a value for the specimen fracture strength at a given strain rate, calculating the incident/reflected and transmitted waveforms, and comparing these waveforms with the experimental traces. These steps are elaborated further in the following.

Step 1: A finite element model is used to calculate for a given test with assigned impact stress history, the incident/reflected and transmitted wave histories, along with specimen average stress and strain histories. The specimen strain rate achieved in the test is also calculated.

Step 2: A cut-off specimen strength at the calculated strain rate is assumed, usually greater than the known quasi-static specimen strength. At this assumed strength the corresponding specimen loading time to fracture is obtained from the calculated specimen stress-time history. This stress-time history will be released from the specimen when it fractures, and hence used as an impacting compressive wave loading for both input and output bars; the traveling waves along two bars due to this loading are calculated in another numerical simulation. In addition, a check on the uniformity of specimen deformation is performed. The number of reverberations (travel between the two specimen faces) of the traveling wave should be at least 10, to assure uniformity.

Step 3: A numerical run is performed for the SHPB using the initial loading wave till the time of fracture obtained from the previous step, in order to obtain the transmitted wave history before the fracture of the specimen.

Step 4: After the fracture of the specimen, the remaining part of the initial loading wave will reflect back from the free end of the input bar as a tensile wave. Thus, in order to calculate this reflected wave history, a separate numerical simulation for the input bar is performed by assuming its ends as free. The load applied in this case is equal to the initial impact stress history used in step 1, but the results considered after the fracture time of the specimen obtained from step 2.

Step 5: Since all traveling waves are elastic, the principle of superposition may be applied. Waves sensed at a particular location on the input and output bars from the previous separate simulations are therefore added up in order to calculate a composite resultant history. This is next compared with the experimental test results at the same locations in question. Qualitative as well as quantitative comparisons are made. If serious deviations exist, a new iteration is performed with different cut-off specimen strength. Steps 2 to 5 are repeated until agreement is obtained between the two results from simulation and experiment.

This exercise helps revealing the value of the specimen strength at the given strain rate. For other strain-rates, tests are usually performed at different specimen lengths and/or impact load. Steps 1 to 5 are then repeated.

The procedure described above is presented in the flow chart of Fig. 4.1, and applied in detail in the following sections. The whole spectrum of traveling waves along the input and output bars is also clarified using the x-t characteristic diagram of Fig. 4.2

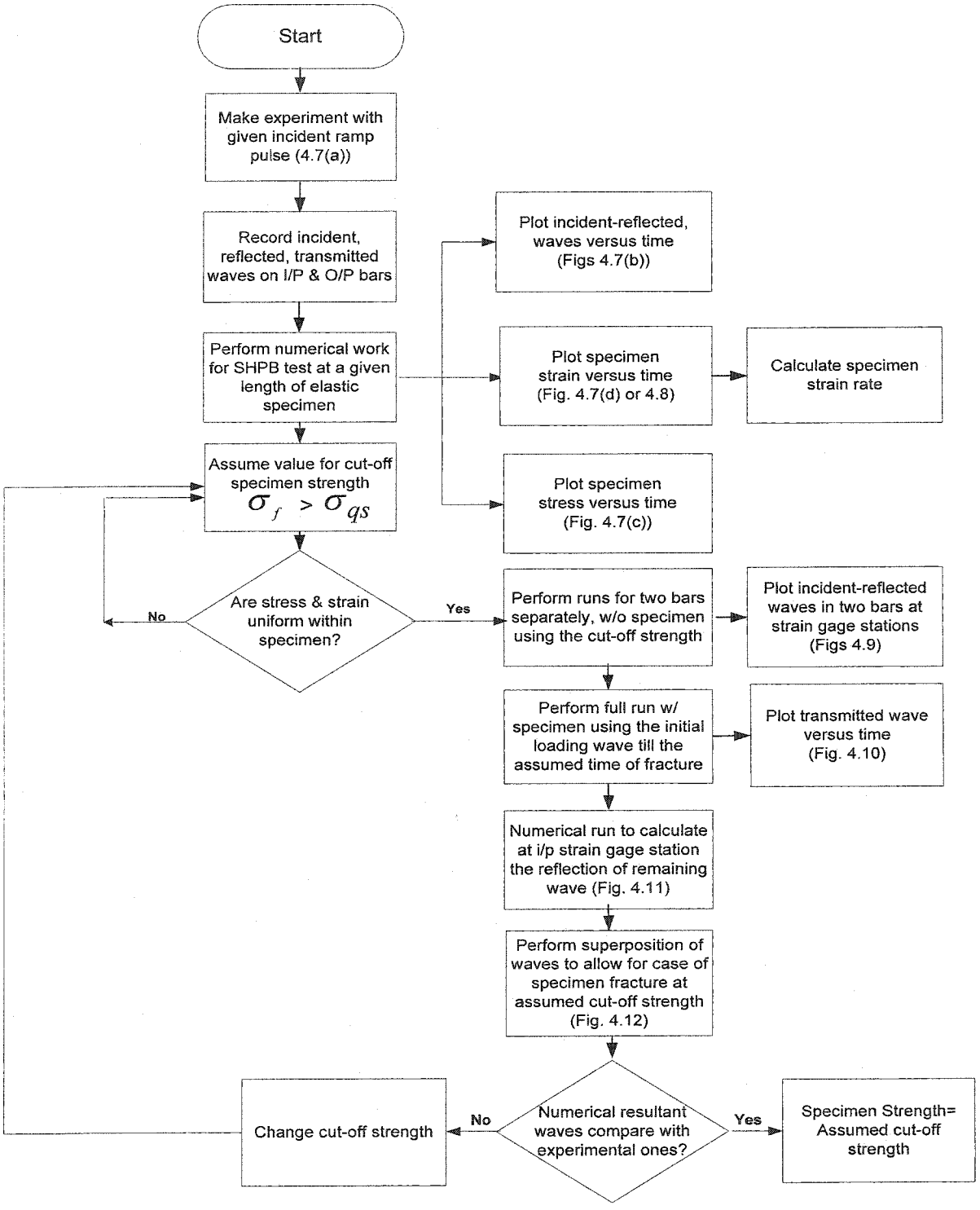

Fig. 4.1 Flow chart for determination of specimen strength and strain rate

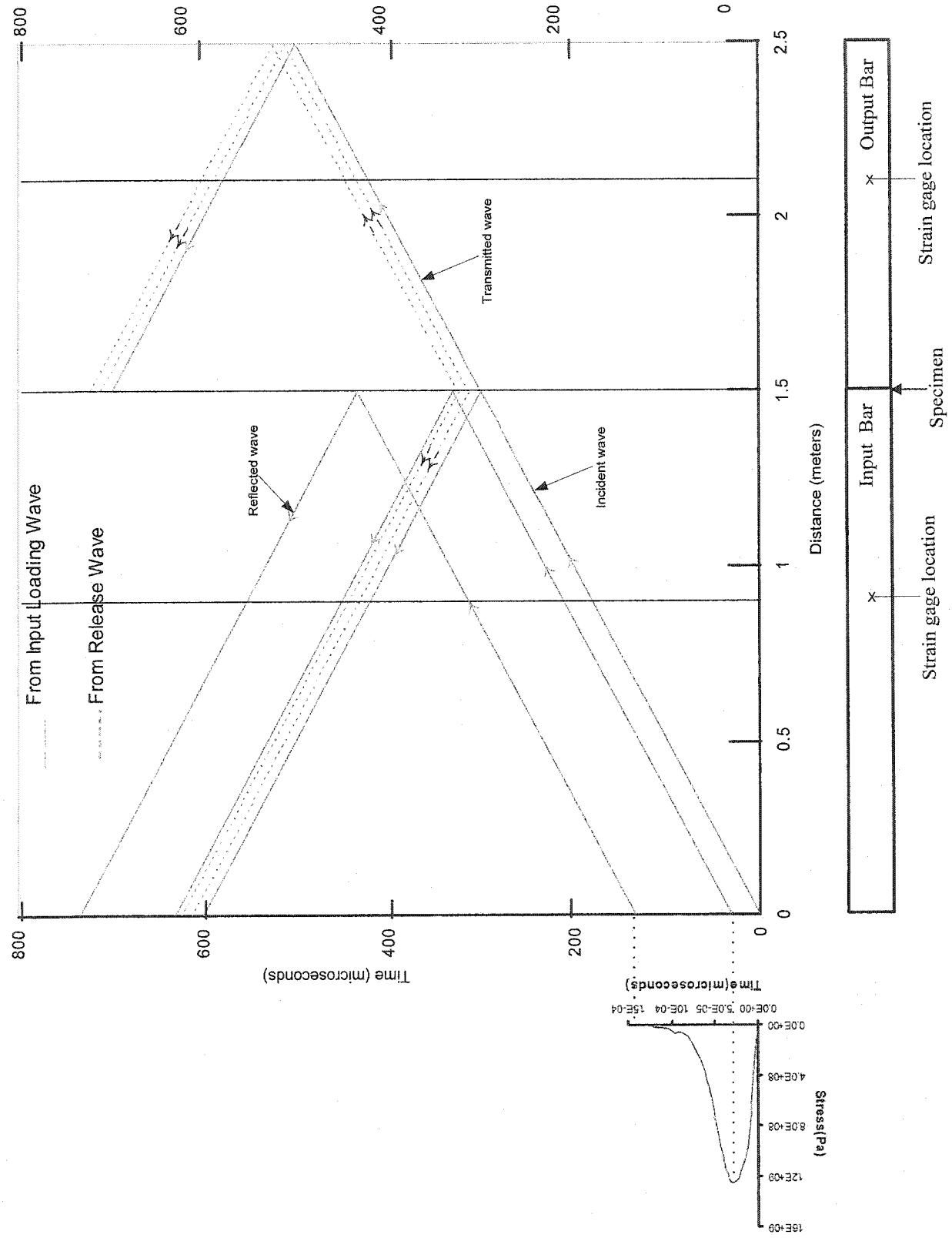

Fig. 4.2 Characteristic x-t diagram

4.3 General Descriptions of the Software Used

The numerical simulation and resulting computations were performed using a finite element analysis with ANSYS software program as a vehicle.

The ANSYS program has many finite element analysis capabilities, ranging from a simple, linear, static analysis to a complex, nonlinear, transient dynamic analysis, but for large deformation dynamics, quasi-static problems with large deformations and multiple nonlinearities, and complex contact/impact problems, ANSYS combines with LS-DYNA explicit finite element program with the powerful pre- and post processing capabilities of the ANSYS program.

The explicit method of solution used by LS-DYNA provides fast solutions for short-time, large deformation dynamics, quasi-static problems with large deformations and multiple nonlinearities, and complex contact/impact problems. Using this integrated product, one can model the structure in ANSYS, obtain the explicit dynamic solution via LS-DYNA, and review results using the standard ANSYS post processing tools.

The procedure for an explicit dynamic analysis is similar to any other analysis that is available in the ANSYS 6.1 program.

A typical finite element analysis on ANSYS/LS-DYNA has three distinct steps:

a. Building the Finite Element model
b. Applying loading and obtaining solution
c. Reviewing the results

Details of these three steps are given in Appendix D

4.4 Implementation of the New Approach

The experimental setup and results of Sarva and Nemat-Nasser (2001) will be used in this section to illustrate the implementation of the proposed approach. The specimen tested experimentally for dynamic compressive strength was made of Silicon Carbide. The input and output bars were made of steel (Nemat-Nasser, Isaacs and Starrett 1991). Configuration details of the experimental setup along, along with the results reported are presented in the following sections. The experimental results include the time resolved voltage output received from strain gauges attached on the input and output bars (Fig. 4.3) and the effect of strain-rate on the compressive failure strength of silicon carbide (Fig. 4.4).

4.4.1 Details of the experimental setup

Not all geometric details were given in the paper except for the diameter of the bars, which is equal to 12.7 mm. Therefore, some deductive work was necessary to understand the test configuration used. The x-t characteristic diagram of Fig. 4.2 was also helpful in that respect. The lengths of the bars were calculated from the traces given for the time resolved voltage output received from the strain gauge bridges attached on the input and output bars for a sample test (Fig. 4.3). As can be seen, the reflected and transmitted traces start at the same time. This indicates that the strain gauge stations were located at equal distances from the specimen.

Therefore, the distance from the specimen/bars interfaces to the location of the strain gauges on the incident and transmitted bars, denoted by d_a, was calculated from

$$d_a = ct_a / 2$$

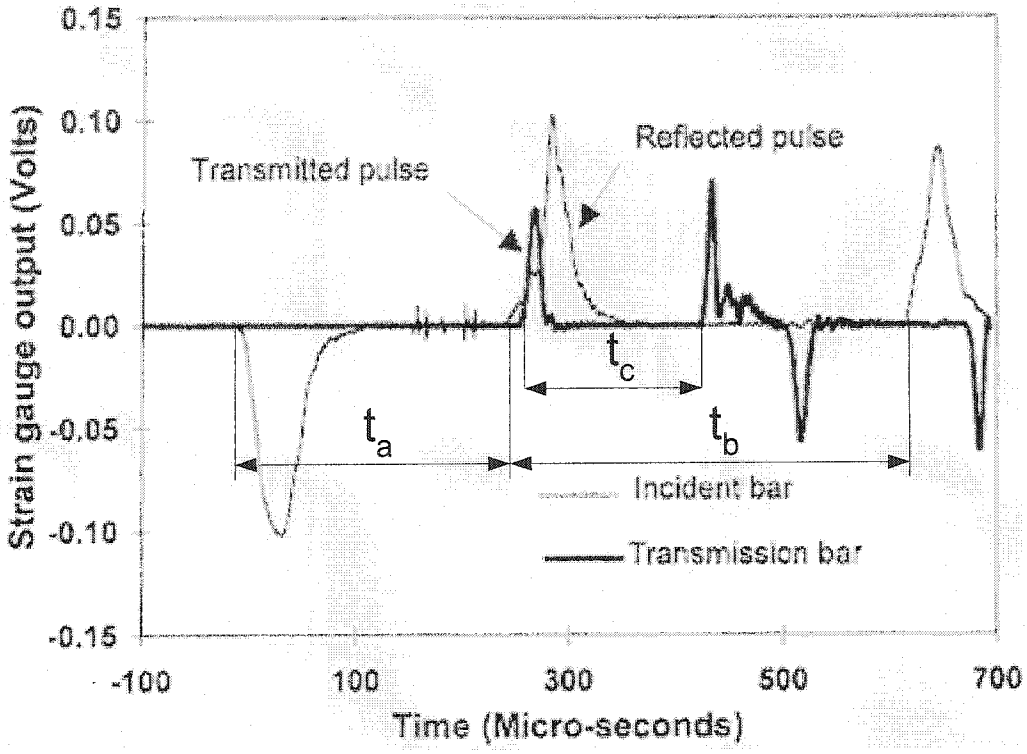

Fig. 4.3 Experimental traces obtained from strain gauges on I/P and O/P bars (Sarva and Nemat-Nasser, 2001)

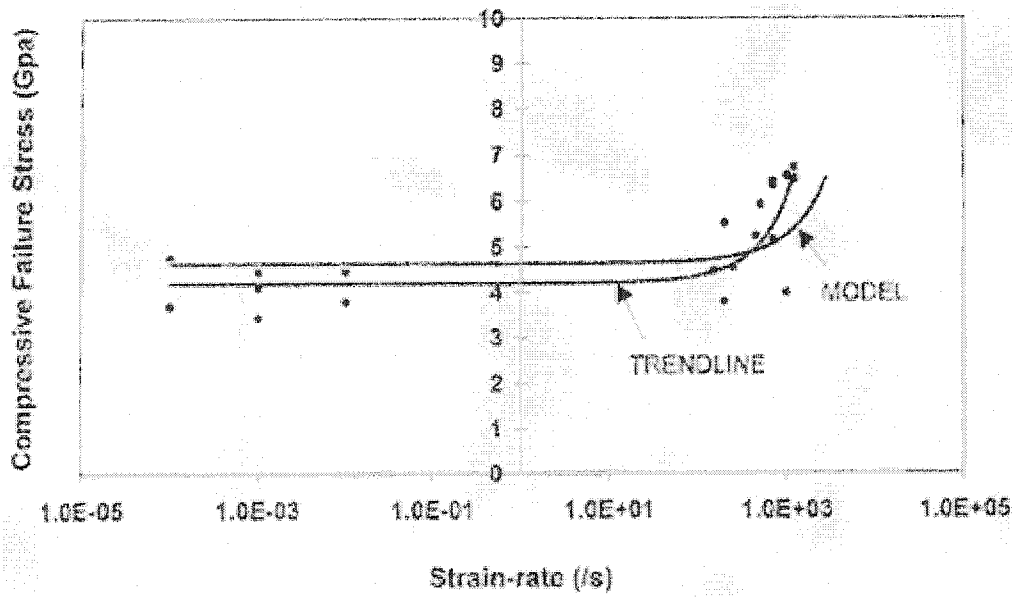

Fig. 4.4 Experimental results for compressive failure strength (Sarva and Nemat-Nasser, 2001)

where, c is the longitudinal wave speed in the steel bars which is equal to $5000m/s$ and t_a is the time taken by the wave to travel from the strain gauge station on the input bar to specimen/input bar interfaces and back, t_a is equal to 250 μs as shown in Fig. 4.3. Thus

$$d_a = \frac{5000\left(\frac{m}{s}\right)\times 250\times 10^{-6}(\mu s)}{2} = 0.625m$$

Therefore the distance between the specimen/bars interfaces to the two strain gauge locations on the input and output bars was taken as 0.6 meters.

The remaining lengths of the input and output bars were calculated as follows. The distance from the impact end of the incident bar to its strain gauge location, denoted by d_b was obtained from:

$$d_b = ct_b$$

where, t_b is the time taken by the elastic wave to travel twice the distance between the impact end and the strain gauge location as shown in Fig. 4.3. Therefore:

$$d_b = \frac{5000\left(\frac{m}{s}\right)*360(\mu s)}{2} = 0.9m$$

Also:

$$d_c = ct_c$$

where d_c is the distance from the strain gauge location on the transmitted bar to its farthest fixed end from the specimen and t_c is the time taken by the elastic wave to travel twice that distance, as shown in Fig. 4.3. Therefore

$$d_c = \frac{5000\left(\frac{m}{s}\right)*160(\mu s)}{2} = 0.4m$$

Based on these calculations, the total lengths of the bars as used in the numerical simulation were 1.5 meter for the input bar and 1.0 meter for the output bar.

4.4.2 Numerical Model

(a) Idealization

The SiC specimens used in the experiments were of length 6.35 mm and of a square cross-section 3.5 by 3.5 mm. In the simulation, the geometry was idealized to be cylindrical of length 6.35 mm and diameter 3.175 mm. Since the symmetry with respect to geometry and loading exists about the axis of the two cylindrical bars and the specimen in the SHPB setup (y-axis is in model), it can be modeled by considering axisymmetry. PLANE 162 elements (ANSYS/LS-DYNA) with axisymmetric option are considered. The element is defined by four nodes having six degrees of freedom at each node: translations, velocities, and accelerations in the nodal x and y directions. Since the bars will be elastic in nature throughout the test, and also the specimen under test will behave linearly till fracture due to its brittle nature, the material properties used for the bars and specimen are those of linear elastic materials.

(b) Finite Element Model

***Geometry*:** Now the 3D problem is reduced to 2D due to axial symmetry, with three rectangles only; the geometric representation is shown in Fig. 4.5.

***Material Properties*:** Linear isotopic properties for bars (Steel) and specimen (Silicon Carbide) are specified using two different models (ANSYS/LSDYNA); these are listed in Table 4.1.

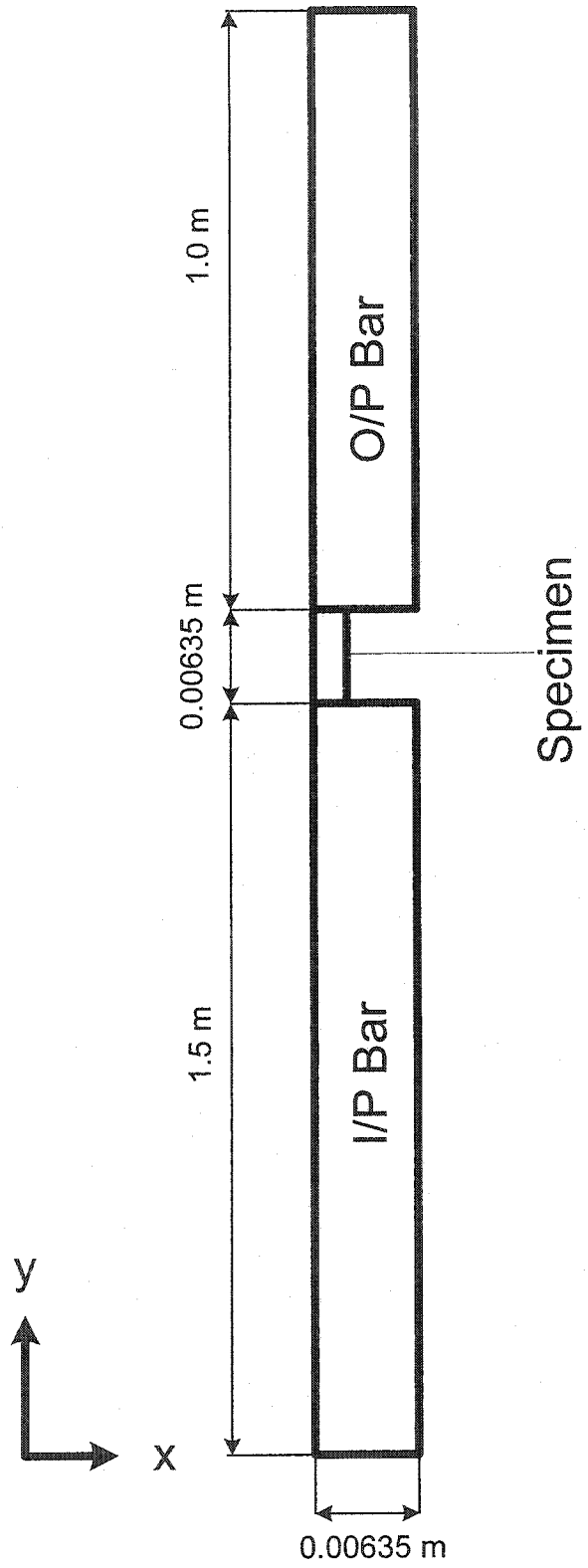

Fig. 4.5 Geometric representation of the axisymmetric model of SHPB (not to scale)

***Meshing*:** Careful consideration had been given while meshing the model for bars and specimen. Meshing used is shown in Fig. 4.6. It is refined for more accuracy, because as a general rule, the finer the FE mesh, the more accurate the results. The number of elements used in the model was 2016 and 2880 for the specimen, and each bar, respectively.

***Contact*:** After meshing the geometry, the contact is applied at the specimen- bars interfaces with the help of Single Surface Auto 2-d option (ANSYS/LSDYNA).

***Boundary Conditions*:** The next step after building the geometric model is applying boundary conditions. The constraint in the form of roller support is applied due to the axial symmetry, i.e. line x=0 is constrained in x and allowed to move in y.

***Loading*:** The loading conditions for the explicit dynamic analysis were determined from the experimental data traces of the incident stress versus time history as presented in Fig. 4.7 (a). The load is applied in the form of pressure.

4.4.3 Input data values

For verification of the developed FE programs, the traces given (Sarva and Nemat-Nasser, 2001) for the dynamic compressive strength of silicon carbide at a strain rate of 1200/sec were simulated. The configuration of the setup was as presented in the previous section, and the material properties were as provided in the paper and shown in Table 4.1. The quasi-static strength of SiC as reported was 4.2 GPa at 250 s^{-1}.

Table 4.1 Data used in the numerical analysis

Material properties	**Geometric properties**
I/P & O/P bars: linear elastic	**I/p bar**
Modulus of elasticity=200GPa	Length=1.5meter
Poisson ratio=0.3	Diameter=0.0127meter
Density=7860Kg/m^3	**O/p bar**
Specimen: linear elastic	Length=1.0meter
Modulus of elasticity=500GPa	Diameter=0.0127meter
Poisson ratio=0.2	**Specimen**
Density=4535Kg/m^3	Length=0.00635meter;
Quasi-static strength=4.2 GPa	Diameter=0.0035meter

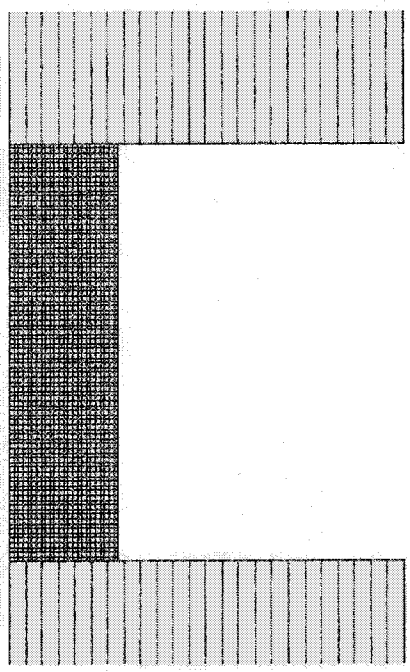

Fig. 4.6 FEM model of specimen and portion of pressure bars

4.4.4 Numerical Runs

Numerical computations were performed for the case of interest as presented in Fig. 4.3. The experimental traces obtained at 1200 s^{-1} by Sarva and Nemat-Nasser (2001) was simulated by using the exact loading conditions and configuration of setup in order to check the validity of the developed numerical model. After obtaining the reasonable closeness between the given experimental results and the obtained numerical ones, other numerical computations can be performed in order to see the effect of specimen length and amplitude of input stress on the strain rate, and compared with experimental data, if available.

The results of the computations will now be presented.

(A) First Trial

Step 1: The experimental traces presented by Sarva and Nemat-Nasser (2001) at the strain rate of 1200/sec were simulated by using the configuration of the setup presented in section 4.4.1. The incident trace given at a rise time of approximately 30 μs as shown in Fig. 4.7(a) is used as the ramp loading for this numerical work, with a maximum stress amplitude of 1250MPa, which was found, by trial and error, suitable to achieve the specimen strain rate of about 1200 s^{-1}. Fig. 4.7 also presents the obtained incident/reflected wave histories at the strain gauge locations in the input (b) bar, along with the stress (c) and strain (d) histories at the mid of the specimen. The corresponding strain rate achieved in this numerical run was calculated from the strain-time history obtained at the mid-section of the specimen, Fig. 4.7(d). As shown in Fig. 4.8, the expansion of Fig. 4.7 (d), it was found equal to 1240/sec in this case, almost equal to the experimental result reported.

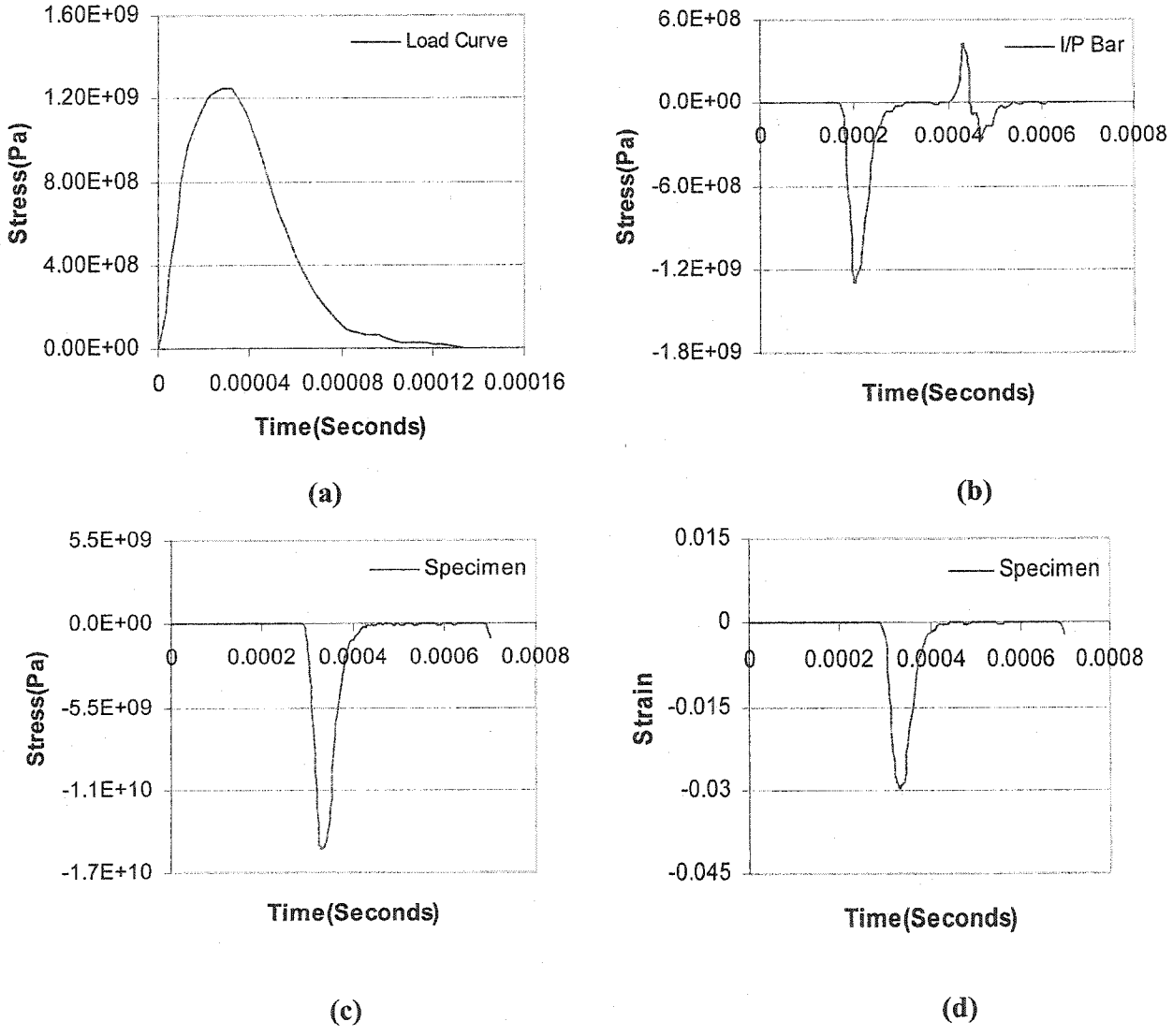

Fig. 4.7 Stress/strain histories for step1 (i.e. complete run for SHPB at a given impact stress history) at specimen fracture strength of 6 GPa

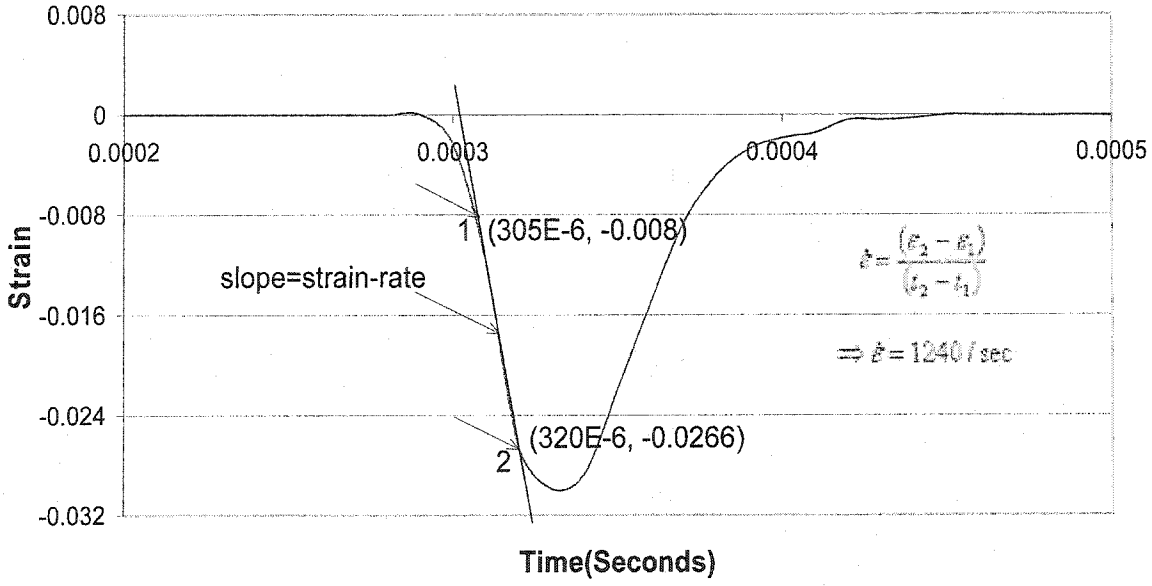

Fig. 4.8 Strain history at the middle of the specimen

Step 2: As a first trial, a cut-off specimen strength greater than the quasi-static strength of 4.2 GPa, is assumed to be 6 GPa. At this strength the corresponding specimen loading time to fracture is estimated at 10 μs from the calculated specimen stress-time history, Fig. 4.7 (c). This stress-time history at specimen fracture is used to calculate the corresponding release compressive wave, loading both input and output bars as shown in Fig. 4.9; this form, in effect, step 2 in the simulation. The maximum stress amplitude of 228 MPa used for loading both input and output bars was calculated from:

$$\sigma_b = \frac{\sigma_s A_s}{A_b} = \frac{\frac{6000(MPa)}{2} * 3.5^2(mm^2)}{12.7^2(mm^2)} = 227.8MPa$$

where, σ_b is the bar stress, A_b is the cross-sectional area of the bar (12.7*12.7 mm^2), σ_s is the assumed specimen cut-off strength (6000 MPa) and A_s is the cross-sectional area of the specimen (3.5*3.5 mm^2). The shape of the loading wave used in this case is shown in Fig. 4.9, includes a loading and unloading time of 10 micro-seconds (as discussed above) with the maximum amplitude of 228 MPa. From these runs, the resulting traveling waves along the bars are calculated, and those related to the strain gauge stations are shown in Fig. 4.9.

Step 3: In order to calculate the transmitted wave history in the output bar till the fracture time of the specimen, a separate run for complete SHPB had been performed using the initial loading wave till the time of fracture. The loading wave along with the wave history obtained at the strain gauge location of the output bar is shown in Fig. 4.10 (a) and (b). The maximum stress amplitude used for loading in this case is 800 MPa, was taken from the initial loading wave shown in Fig. 4.7(a) till the fracture time of the specimen,

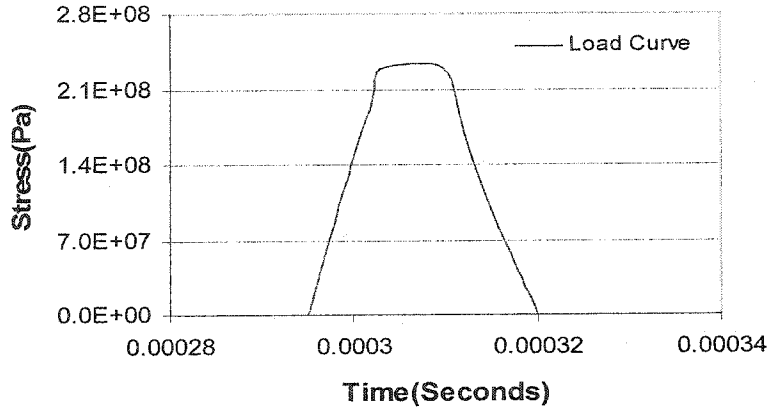

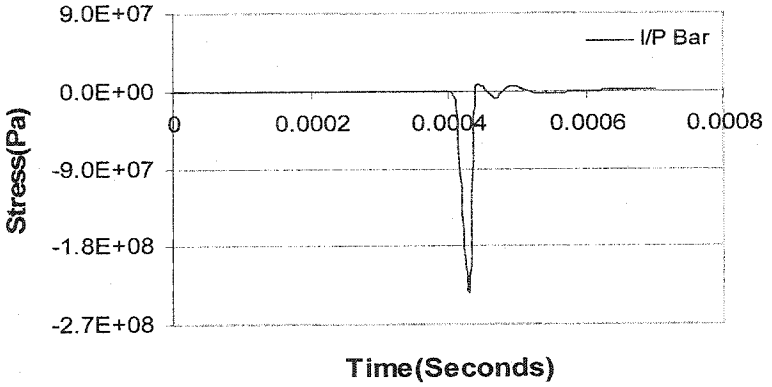

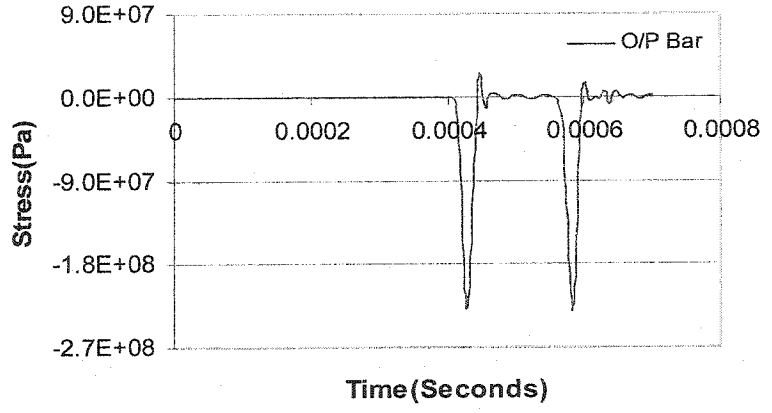

Fig. 4.9 Stress histories for step2 (i.e. separate runs for input and output bar, in order to calculate the release wave) at specimen fracture strength of 6 GPa

i.e. 10 micro-seconds. Here also, the shape chosen is shown in Fig. 4.10 (a), which includes a loading and unloading time of 10 micro-seconds.

Step 4: After fracture of the specimen, the remaining part of initial loading wave will reflect back from the "now" free end of the incident bar as a tensile wave. Thus in order to calculate this reflected wave history, a separate numerical simulation for the input bar is performed by assuming its end as free. This constitutes step 4 in the simulation. The load applied in this case is equal to the initial impact stress history used in step 1 as shown in Fig. 4.11 (a). The wave history at the strain gauge location of the input bar is shown in Fig. 4.11 (b). However, only the portion of that history corresponding to time following specimen fracture, which is equal to 440 μs, is considered for the next step (step 5) where the superposition of all traveling waves in the input bar is performed.

Step 5: Since all traveling waves are elastic, the principle of superposition is applied (step 5). Waves sensed at the strain gage locations on the input and output bars from the four separate simulations are therefore added up in order to calculate a resultant composite history as shown in Fig. 4.12, due account being taken of the proper time in each case, i.e. the initial loading wave reflected from the specimen bar interface is considered till the fracture of the specimen, which is equal to 440 μs, whereas the release wave initiated after the specimen fracture and the remaining part of initial loading wave is accounted after 440 μs. Figure 4.12 is next compared with the experimental test results shown in Fig. 4.13 at the same locations. After making the qualitative as well as quantitative comparisons between the traces of experimental and numerical work, it is found that the calculated reflected and transmitted waves do not correspond to the experimental ones in terms of their shape and relative amplitudes.

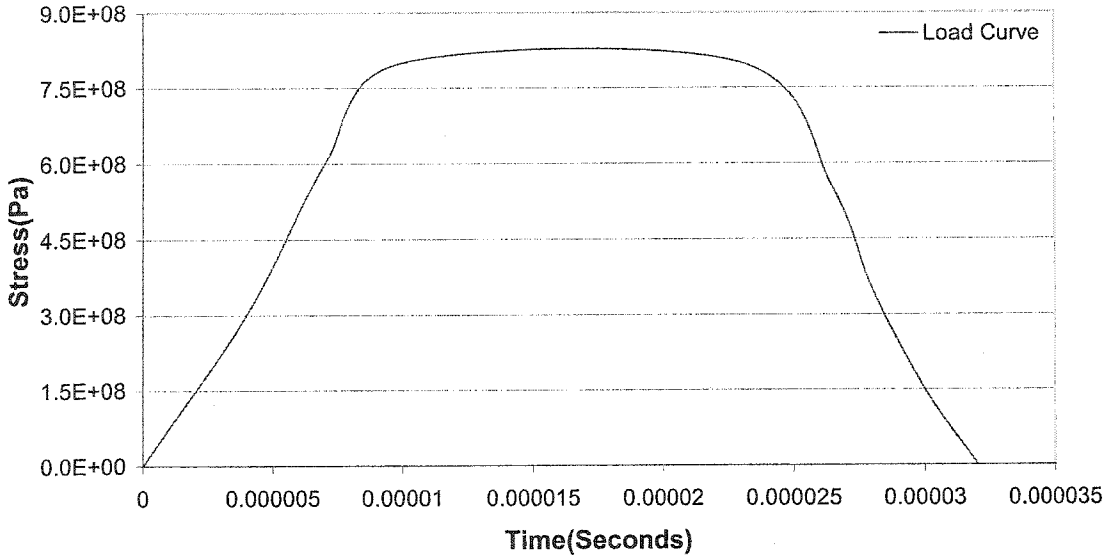

(a)

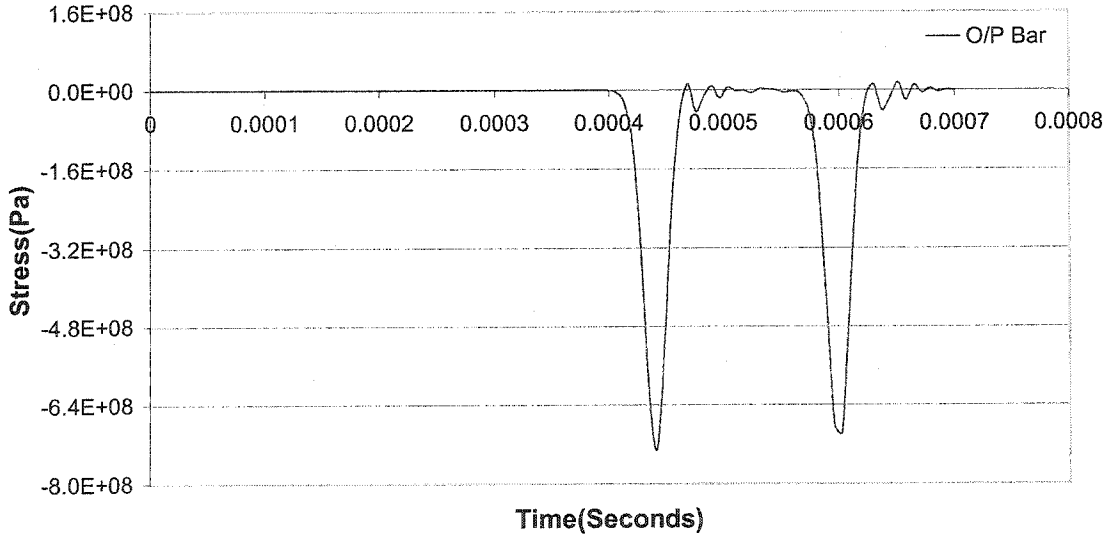

(b)

Fig. 4.10 Stress histories for step3 (i.e. complete run for SHPB using initial loading wave till the time of fracture, i.e. 10 μ_s, in order to calculate stress history for output bar) at specimen fracture strength of 6 GPa

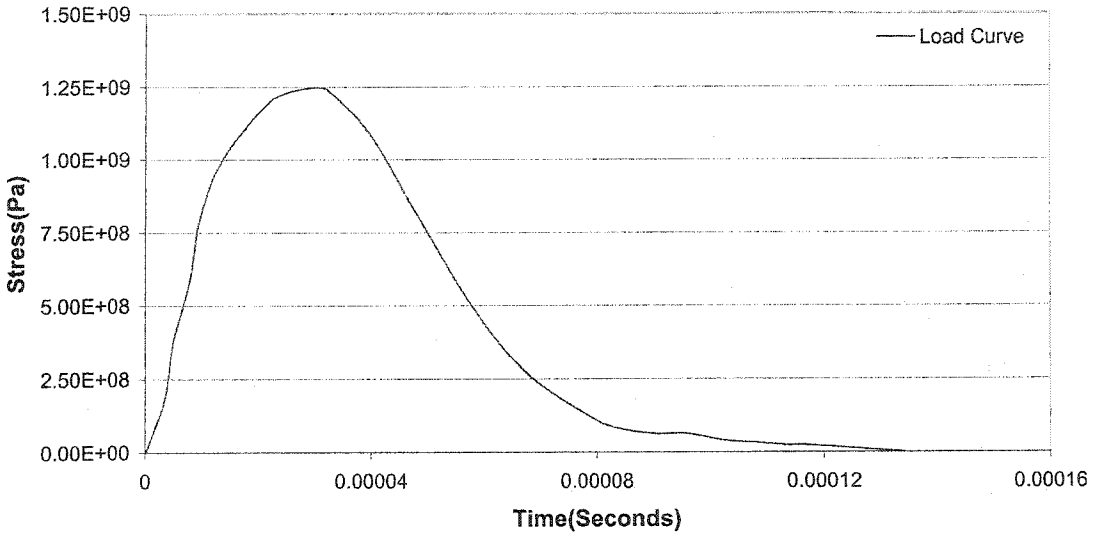

(a)

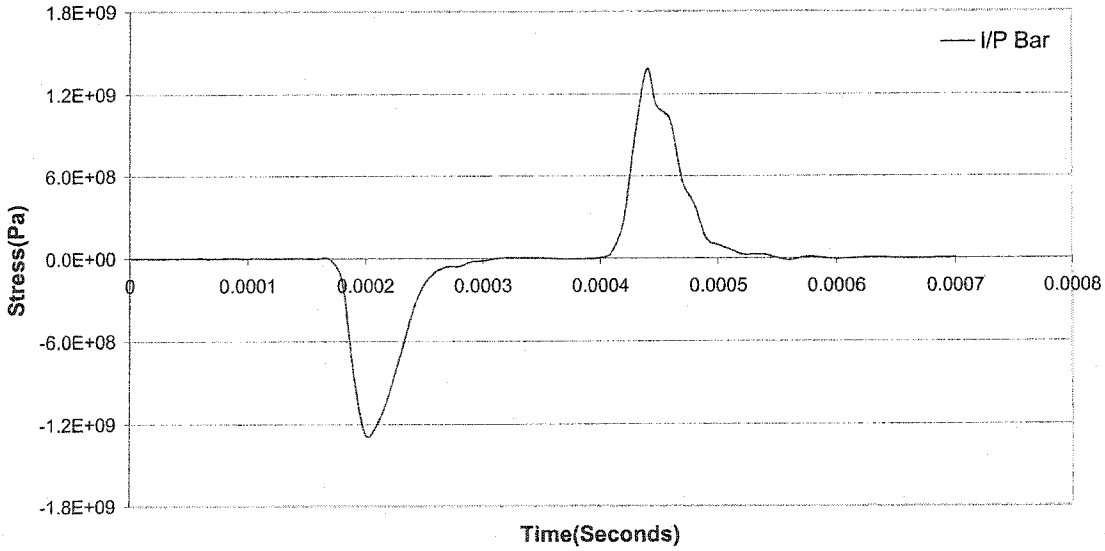

(b)

Fig. 4.11 Stress histories for step4 (i.e. numerical run for input bar using the initial loading wave, in order to calculate the reflected wave after fracture of the specimen) at specimen fracture strength of 6 GPa

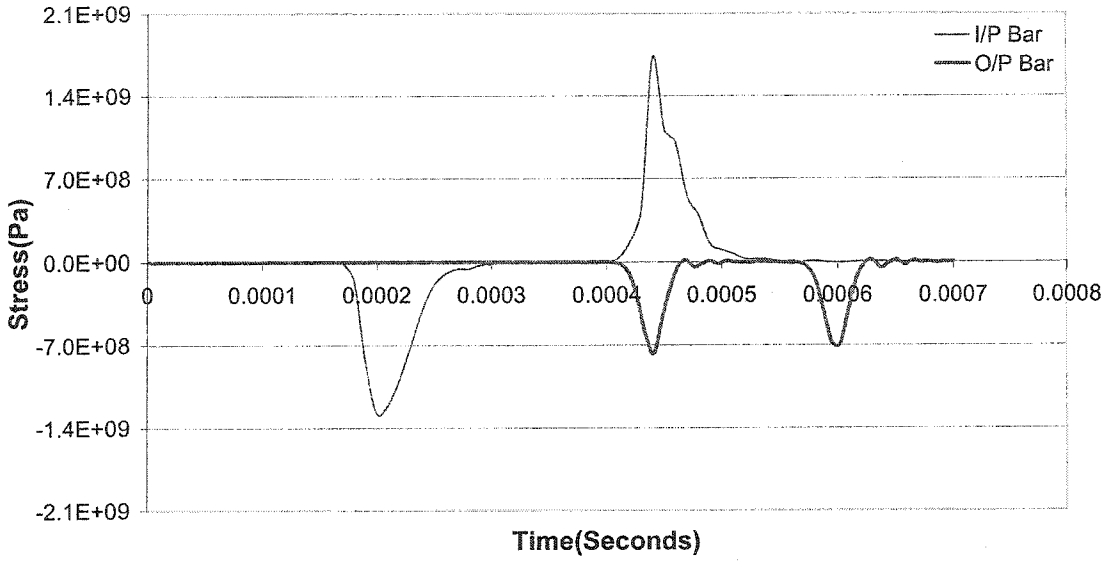

Fig. 4.12 Resultant numerical traces obtained (combination of steps 1-4) at specimen fracture strength of 6 GPa and strain-rate of 1200/sec

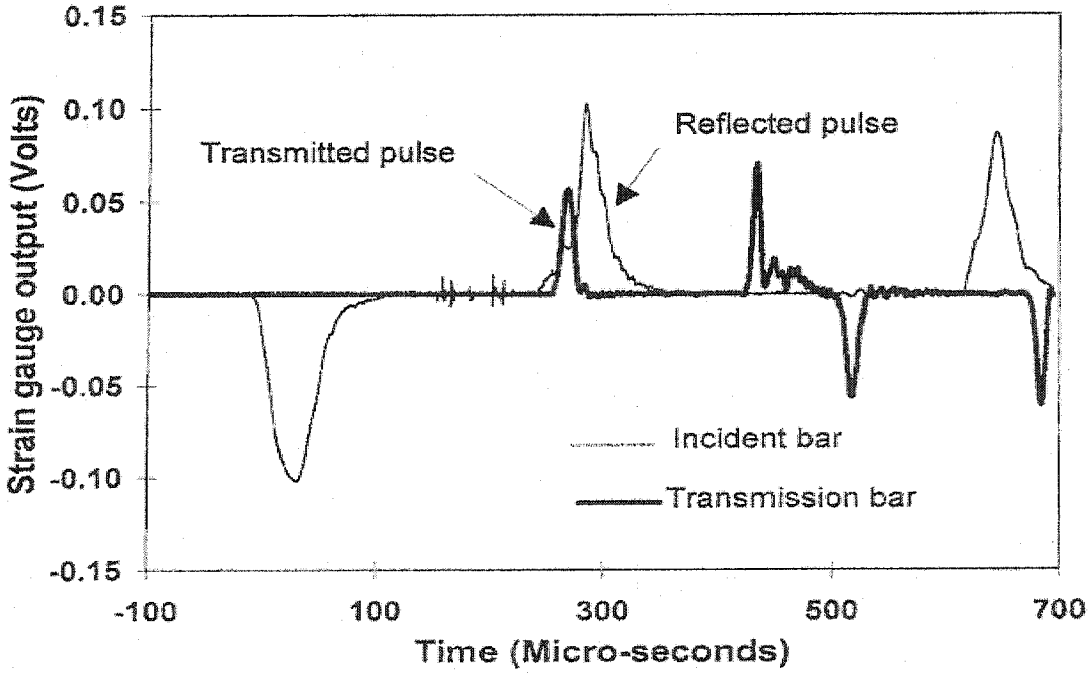

Fig. 4.13 Experimental traces at a strain rate of 1200/sec

It is clear from the obtained results that the assumed cut-off specimen strength of 6 GPa in the current simulation is not the right choice. A second iteration is then performed with a value of 7 GPa.

(B) Second Iteration

Here, a different specimen cut-off strength is assumed, namely 7GPa. In this case, steps 1 and 4 are the same as discussed and presented in the first trial.

Step 1: This step is as presented and discussed in the previous case, in order to guarantee the same specimen strain rate of 1200 s^{-1}, but the cut-off strength of the specimen assumed is different than the previous one, as shown in Fig. 4.14 (c).

Step 2: At the assumed cut-off strength of 7GPa, the corresponding specimen loading time to fracture is estimated from the calculated specimen stress-time history Fig. 4.14 (c), at 12 μs, and the maximum stress amplitude is calculated similarly to that in previous trial, which is equal to 265 MPa in this case. This stress-time history at specimen fracture is used to calculate the corresponding release compressive wave, loading both input and output bars; this form, in effect, step 2 in the simulation, the results of which are shown in Fig. 4.15.

Step 3: As discussed previously, to calculate the transmitted wave history in the output bar till the fracture time of the specimen, a separate run for complete SHPB had been performed using the initial loading wave till the time of fracture, this form, in effect, step 3 in the simulation. The loading wave along with the wave history obtained at the strain gauge location of the output bar is shown in Fig. 4.16 (a) and (b). The maximum stress amplitude used for loading in this case is 970MPa, was taken from the initial loading

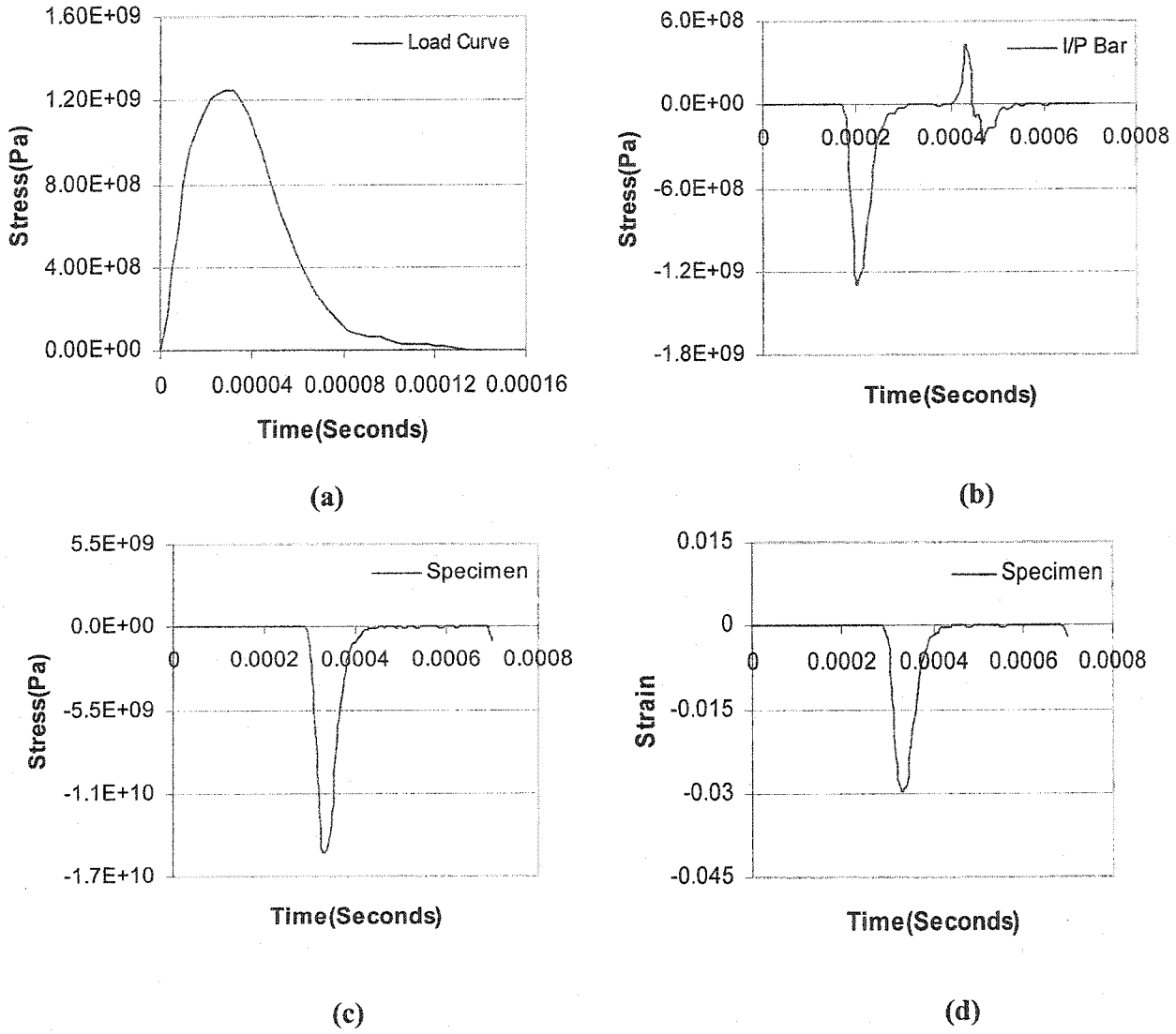

Fig. 4.14 Stress/strain histories for step1 (i.e. complete run for SHPB at a given impact stress history) at specimen fracture strength of 7 GPa.

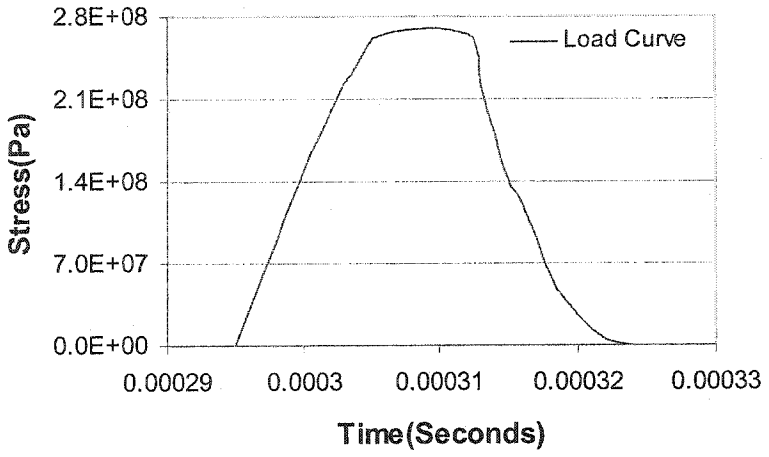

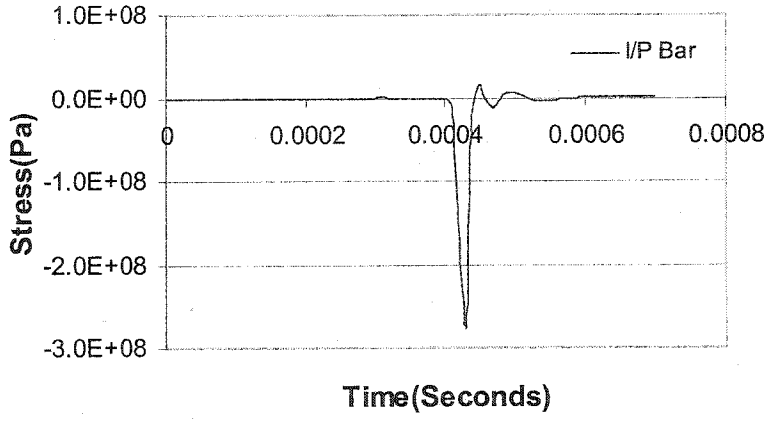

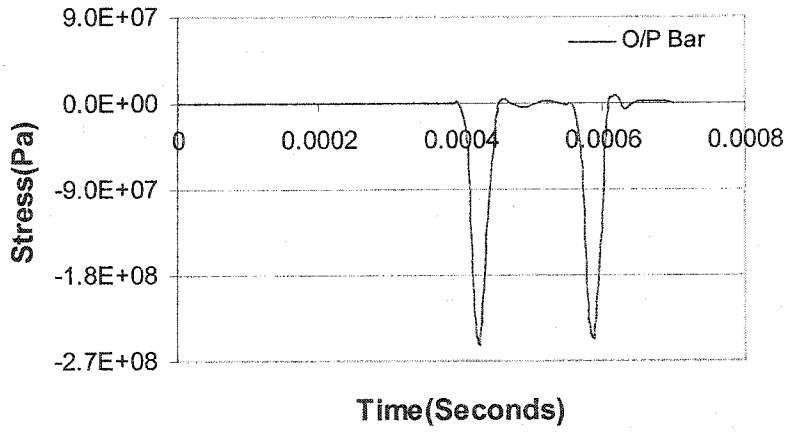

Fig. 4.15 Stress histories for step2 (i.e. separate runs for input and output bar, in order to calculate the release wave) at specimen fracture strength of 7 GPa.

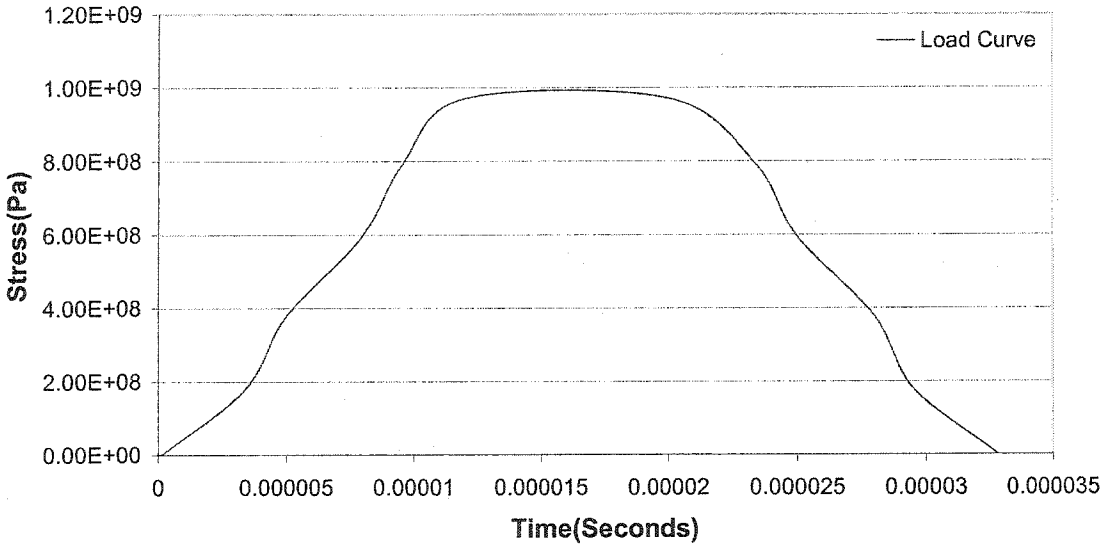

(a)

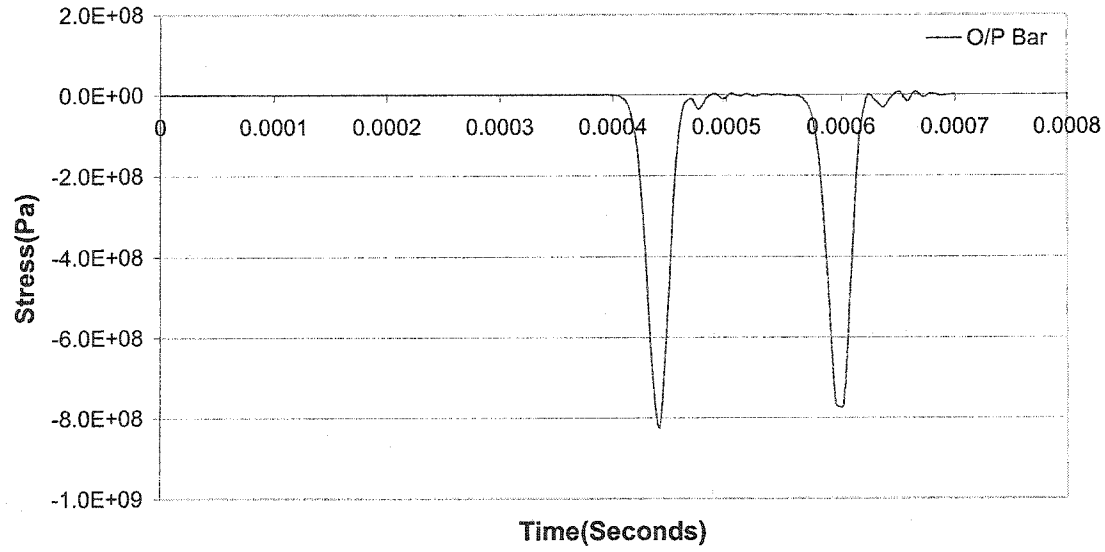

(b)

Fig. 4.16 Stress histories for step3 (i.e. complete run for SHPB using initial loading wave till the time of fracture, i.e. 12 μ_s, in order to calculate stress history for output bar) at specimen fracture strength of 7 GPa.

wave shown in Fig. 4.14 (a) till the fracture time of the specimen, which is equal to 12 micro-seconds.

Step 4: After fracture of the specimen, the remaining part of initial loading wave will reflect back from the "now" free end of the incident bar as a tensile wave. Thus in order to calculate this reflected wave history, a separate numerical simulation for the input bar is performed by assuming its end as free. This constitutes step 4 in the simulation and it is same as presented in the first trial (Fig. 4.17), except the portion (starting at 444 μs) considered for the following step (step 5), where the superposition of all traveling waves in the input bar is performed.

Step 5: Since all traveling waves are elastic, the principle of superposition is applied (step 5). Waves sensed at the strain gage locations on the input and output bars from the four separate simulations are therefore added up in order to calculate a resultant composite history as shown in Fig. 4.18, due account being taken of the proper time in each case.

Figure 4.18 is next compared with the experimental test results shown in Fig. 4.13 at the same locations. Qualitative as well as quantitative comparisons between the two traces show reasonable closeness between the two. Moreover, by comparing the computed resultant reflected and transmitted waves of Fig. 4.18 with the experimental traces shown in Fig. 4.13, the following observations can be made:

a) General

i. The experimental traces are given as strain gage output in volts versus time, whereas the calculated traces show the stress amplitudes versus time. This fact does not

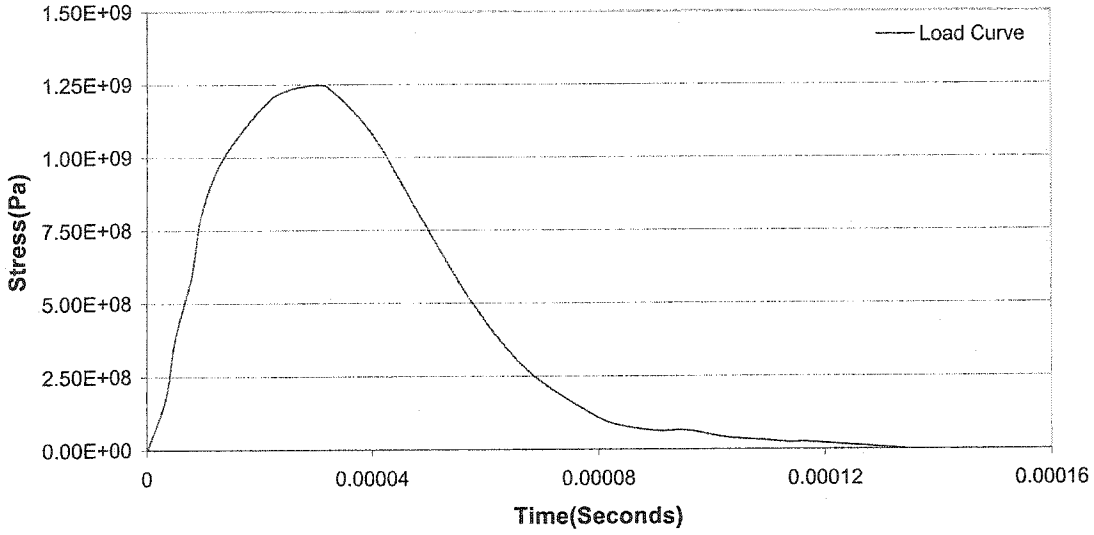

(a)

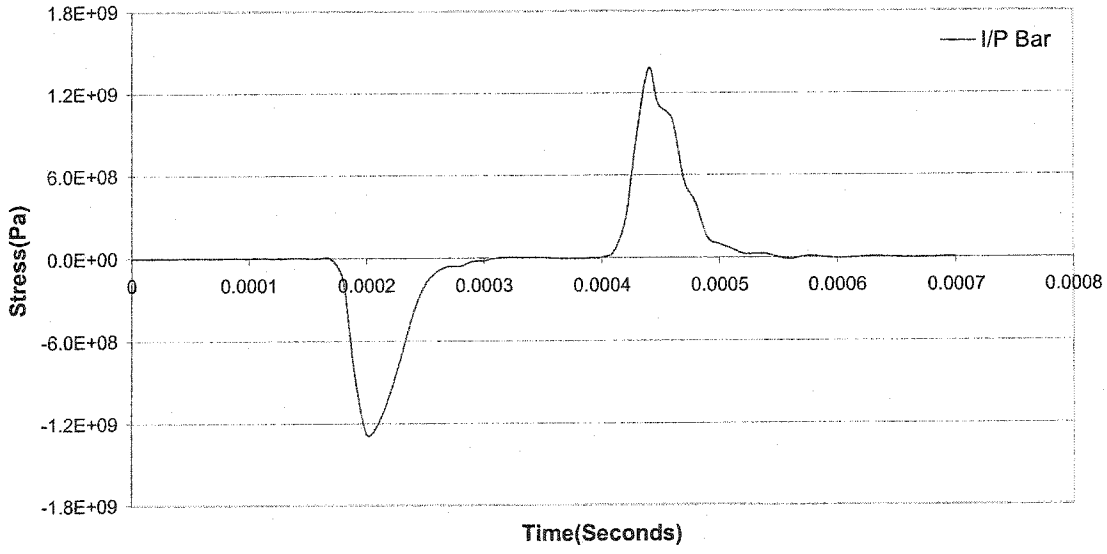

(b)

Fig. 4.17 Stress histories for step4 (i.e. numerical run for input bar using the initial loading wave, in order to calculate the reflected wave after fracture of the specimen) at specimen fracture strength of 7 GPa.

prevent the comparison to be performed. If the strain gauge factors were known, the experimental traces could be multiplied by a constant factor to obtain stresses.

ii. The timescale shown in the experimental traces starts with zero at the input bar gage station, whereas in the calculations zero time starts at impact end of the input bar.

The transmitted wave is shown upward in the experimental traces of Fig. 4.13. In fact, these traces should be compressive like the incident wave. The reason behind inverting the inputs to the oscilloscope to obtain the shown transmitted wave is not known, and was not mentioned in the paper by the authors.

b) Reflected Waves

The reflected waves obtained through calculation (Fig. 4.18) are identical to the experimental ones (Fig. 4.13). Both consist of three different behaviors such as:

1. Reflection of the certain portion (up to specimen fracture) of initial loading wave from the input bar-specimen interface.
2. The release wave from the specimen which initiates after its fracture.
3. The remaining part of the loading wave which reflects off from the "now" free end of the input bar, after the fracture of the specimen.

Also, the maximum amplitude of the reflected wave is about 99% of the incident wave from the experiment, and about 92% of the incident wave from calculation.

c) Transmitted Waves

As seen in the two figures, the calculated and experimental transmitted waves are almost identical. The maximum amplitude of the wave is about 59% of the incident wave from the experiment, and about 64% of the incident wave from calculation.

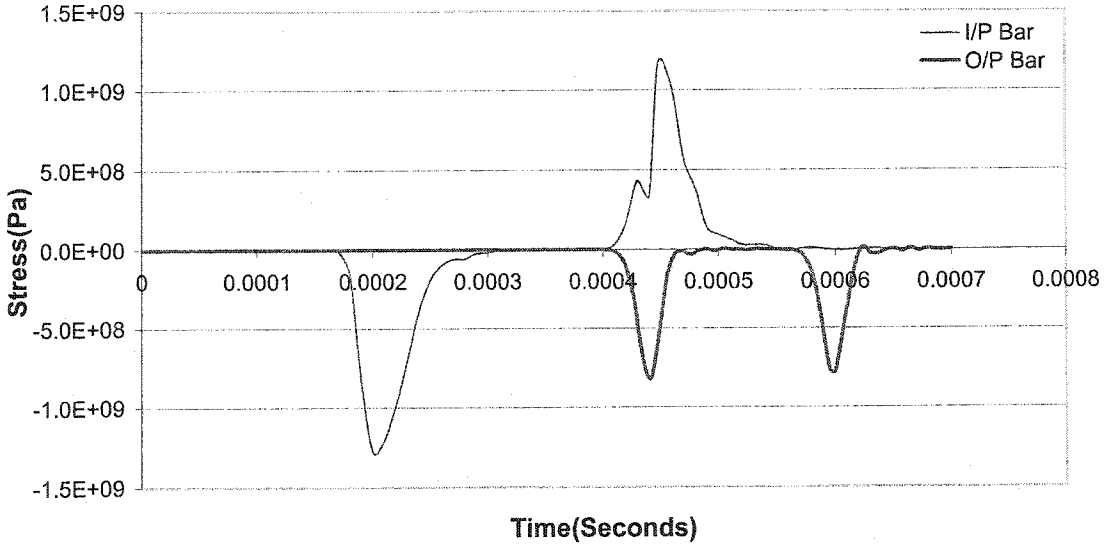

Fig. 4.18 Resultant numerical traces obtained (combination of steps 1-4) at specimen fracture strength of 6 GPa and strain-rate of 1200/sec

The experimental traces show the reflection of the transmitted wave from the specimen-output bar interface (now a free end) as can be seen in the x-t diagram of Fig. 4.2. This is not shown in the calculated traces because the calculations were carried out only up to 700 μs from the start of impact on the input bar.

In conclusion, it is clear that the numerical simulation approach detailed in this Chapter can closely reproduce the traces obtained experimentally. The method should prove to be a straightforward and logical approach to the analysis of SHPB testing of brittle materials.

CHAPTER 5

CONCLUSIONS & RECOMMENDATIONS

5.1 Conclusions

The objective of this thesis was to develop a straightforward methodology to obtain strain rate effect on the strength of brittle materials using the SHPB technique. The following conclusions can be made from the current work.

1. Based on a thorough and critical review of the literature, two important modifications are proposed, namely:

(a) The introduction of a slowly rising compressive pulse followed by a tensile one can be achieved using a sphere as the medium of impact on a cylindrical bar. The resulting impact wave was found to be a smoothly increasing compressive pulse followed by an unloading tensile one. The results were substantiated with a theoretical analysis of different diameter spherical balls hitting a long cylindrical bar of given diameter.

(b) The numerical simulation of the test is possible, by accounting for the specimen fracture and the numerous waves propagating along the input and output bars. This allows for the reconstruction of the resultant reflected and transmitted waves. This approach proved to be feasible when the calculated traces are compared with the experimental ones.

2. The compressive failure strength of brittle materials, here exemplified by SiC, as affected by strain rate is possible to identify using the new numerical simulation approach.

5.2 Recommendations for Future Work

1. The new experimental approach can be used for testing weak brittle materials. For harder materials, it should be enhanced in order to provide a higher input energy. This can be achieved by imparting a higher velocity to the ball using a gas gun.
2. The experimental setup built and instrumented in the present work can be used in the future to generate new data on brittle materials following the important modifications proposed in the current thesis.

REFERENCES

Al-Mousawi, M.N., Reid, S.R., and Deans, W.F., "The use of the split Hopkinson pressure bar techniques in high strain rate materials testing," Proc. Instn. Mech. Engrs. Vol. 211 Part C, (1997)

Barton, C.S., Volterrra, E. G., and Citron, S. J., "On elastic impacts of spheres on long rods. Prpc.3rd U.S. Natn. Cong. App. Mech. 89-94 (1958)

Christensen, R.J., Swanson, S. R., and Brown, W. S., "split-Hopkinson-bar tests on rock under confining pressure", Experimental Mechanics, 29, 508-513 (1972).

Ellwood, S., Griffiths, L. J., and Parry, D. J., "Materials testing at high constant strain rates," J. Phys. E: Sci. Instrum., 15, 280–282 (1982).

Eleiche, A.M., "A literature survey of the combined effects of strain rate and elevated temperatures on the mechanical properties of metals", Technical Report., AFML-TR-72-125, US Air Force Materials Laboratory, Wright-Patterson Air Force Base, Ohio, September 1972.

Field, J.E., Walley, S.M., Bourne, N.K., and Huntley, J.M., "Review of experimental techniques for high rate deformation studies," in 'Acoustics and Vibrations ASIA' 98, 11-13, 9-38 (1998).

Follansbee, P. S., "The Hopkinson bar," in Mechanical Testing, Metals Handbook, 9th ed., American Society for Metals, Metals Park, Ohio, Volume 8, pp. 98–217 (1985).

Franz, C. E., Follansbee, P. S., and Wright, W. J., "New experimental techniques with the split Hopkinson pressure bar," 8th International Conference on High Energy Rate Fabrication, Pressure Vessel and Piping Division, ASME, TX (1984).

Frew, D.J., Forrestal, M.J., and Chen, W., "A split Hopkinson bar technique to determine compressive stress-strain data for rock materials," Experimental Mechanics, 41, 40-46 (2001).

Harding, J., "Material behavior at high rates of strain", in Impact Loading and Dynamic Behavior of Materials, Ed. By C.Y. Chiem, H.D. Kunze, and L.W. Meyer, Springer Verlag, p.23, (1988).

Johnson, W., Impact Strength Of Materials, Edward, London, (1972).

Kaiser, M.A., "Advancements in the split Hopkinson bar test", MS Thesis, Virginia Polytechnic Institute and State University, (1998).

Kolsky, H., "An investigation of the mechanical properties of materials at very high rates of loading", Proc. Phys. Soc. London, B62, 676, (1949).

Kolsky, H., "The stress pulses propagated as a result of the rapid growth of brittle fracture", Engineering Fracture Mechanics, Vol.5, 513, (1973).

Nemat-Nasser, S., Isaacs, J.B., and Starrett, J.E., "Hopkinson techniques for dynamic recovery experiments", Proc. R. Soc. Lond. A 435, 371, (1991).

Nicholas, T., "Material behavior at high strain rates," in Impact Dynamics, Chap. 8, John Wiley and Sons, New York, (1982).

Ravichandran, G., and Subhash, G., "Critical appraisal of limiting strain rates for compression testing of ceramics in a split Hopkinson pressure bar", J. Am. Ceram. Soc, 77(1), 263, (1994),

Sarva, S., and Nemat-Nasser, S., "Dynamic compressive strength of silicon carbide under uniaxial compression", Materials Science and Engineering, A317, 140, (2001).

Sato, Y., and Kikuchi, W., "High strain-rate properties of polymethyl methacrylate", Impact Engineering and Application, Vol. 2, p. 833, Japan (2001).

Shirai, K., Yagishita, T., and Ito, C., "Equations for evaluation of effects of strain rate on concrete mechanical properties", Impact Engineering and Application, Vol. 2, P. 583, Japan (2001).

Togami, T.C., Baker, W.E., and Forrestal, M.J., "A split Hopkinson bar technique to evaluate the performance of accelerometers", J. App. Mech., 63, 353-356 (1996).

Timonshenko, S., and Goodier, J., "Theory of Elasticity", 3rd ed., McGraw-Hill, New York, (1982)

Verleysen, P., and Degrieck, J., "Improved signal processing for split Hopkinson bar tests on (quasi-) brittle materials", Experimental Techniques, Westport, (2000).

Wasley, R.J., Stress wave propagation in solids, Marcel Dekker, Inc. New York, (1973).

APPENDIX A

DERIVATION OF MAIN EQUATIONS USED IN THE SHPB

In the SHPB technique, the specimen is sandwiched between two bars and loaded by a single traveling pulse in compression. The pulse signals are monitored with the aid of strain gauges, and from which the specimen stress, strain rate and strain can be deduced, as discussed in the following sections.

A-1 Specimen stress calculation

The average stress σ_s in the specimen can be obtained from (Al-Mousawi, 1997)

$$\sigma_s = \frac{f_1 + f_2}{2A_s} \tag{A1}$$

where f_1 and f_2 are the applied loads on each face of the specimen as shown in Fig.A_1, and A_s is the specimen cross-sectional area. For a specimen in dynamic equilibrium, f_1 and f_2 are expressed in terms of the input and output pressure bar strains as

$$f_1 = EA_o(\varepsilon_I + \varepsilon_R) \tag{A2}$$

$$f_2 = EA_o\varepsilon_T \tag{A3}$$

where A_0 is the bar cross-sectional area, E the elastic modulus of bar material and ε_I, ε_R and $\varepsilon_T(t)$ are the incident, reflected and transmitted strain histories respectively.

Therefore, the average stress in the specimen is equal to

$$\sigma_s = \frac{EA_O(\varepsilon_I + \varepsilon_R + \varepsilon_T)}{2A_s} \tag{A4}$$

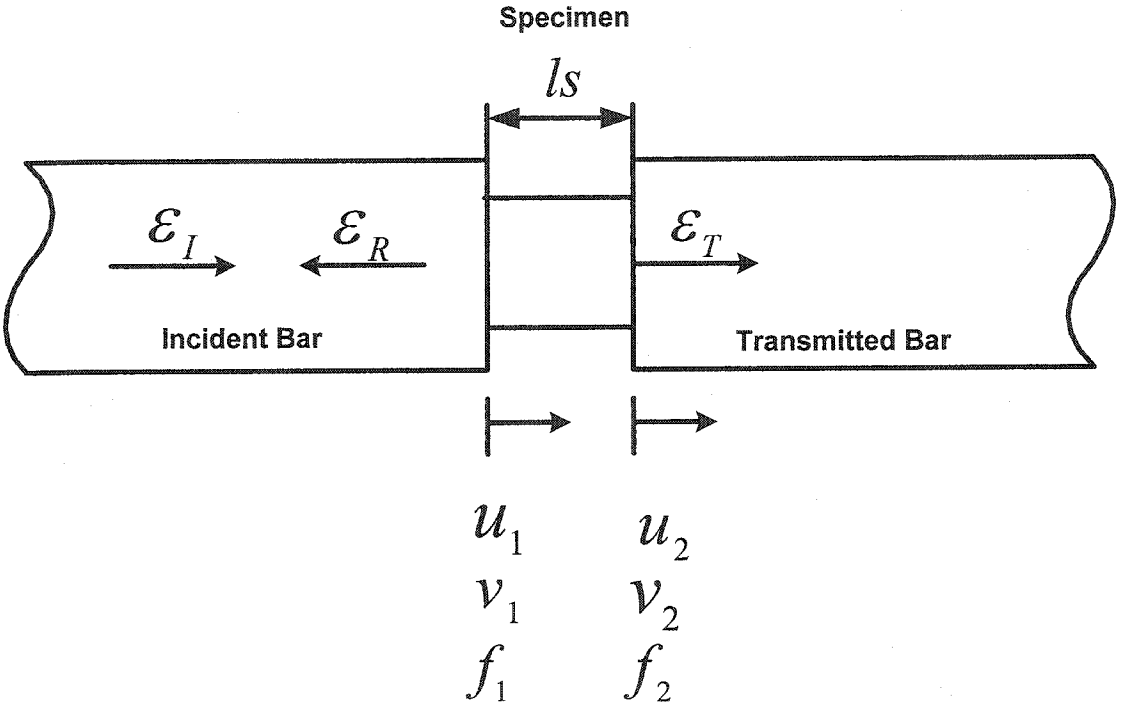

Fig. A_1 Specimen sandwiched between two bars

For a uniformly deforming specimen, the strains in the input bar are equal to the strain in the output bar i.e.

$$\varepsilon_I + \varepsilon_R = \varepsilon_T \tag{A5}$$

Thus, substituting from Eq. (A5) into Eq. (A4) we get

$$\Rightarrow \sigma_S = E\left(\frac{A_o}{A_S}\right)\varepsilon_T \tag{A6}$$

The above equation shows that the stress in the specimen is proportional to the amplitude of the strain transmitted through the specimen into the output bar.

A-2 Specimen strain calculation

The average strain rate in the deforming specimen is given by Al-Moussawi (1996) and Kaiser (1998) as

$$\frac{d\varepsilon}{dt} = \frac{V_1 - V_2}{l_s} \tag{A7}$$

where V_1 and V_2 are the velocities at the input bar/specimen and specimen/output bar interfaces respectively, and l_s is the length of the specimen as shown in Fig. A1.

The velocity V_1 is the product of the longitudinal sound velocity (C_o) in the bar and the total strain at the input bar/specimen interface, which is

$$V_1 = C_o(\varepsilon_I - \varepsilon_R) \tag{A8}$$

Similarly, the velocity at the specimen/output bar interface is given by

$$V_2 = C_o\varepsilon_T \tag{A9}$$

Since in the above equations ε_I, ε_T are compressive strains, they are considered positive, whereas ε_R is a tensile strain, hence considered negative. Therefore, the average strain rate in the specimen is given by:

$$\frac{d\varepsilon}{dt} = \frac{C_o}{l_s}\left[\varepsilon_I - \varepsilon_R - \varepsilon_T\right] \tag{A10}$$

From Eq. (A_5), we have

$$\varepsilon_I + \varepsilon_R = \varepsilon_T \tag{A11}$$

Therefore, substituting in Eq. (A_{10}), we get

$$\Rightarrow \frac{d\varepsilon}{dt} = \frac{-2C_o}{l_s}\left[\varepsilon_R\right] \tag{A12}$$

The above expression can be integrated to yield the specimen strain as

$$\varepsilon = \frac{-2C_o}{l_s}\int \varepsilon_R dt \tag{A13}$$

Thus, the specimen stress and strain are determined simply by measurements made on the elastic bars during the test.

APPENDIX B

ELASTIC IMPACT OF SPHERES ON LONG RODS

The theory of a sphere imparting longitudinal collinear impact on a long cylindrical rod had been discussed in various texts (Barton, Volterra and Citron, 1958; Timoshenko, 1982). The following is a short summary.

Let an elastic ball of mass m and radius r strike the end of an infinitely long cylindrical bar with velocity V_0 in longitudinal impact. Also, let α be the position of center of mass of the ball, γ the position of center of mass of a section of the impacted bar near the point of impact. Then the relative displacement of the centers of mass of ball and bar is β, given by:

$$\beta = \alpha - \gamma \tag{B1}$$

If u represents the elastic displacement of the bar due to impact, then

$$u = \alpha - \beta \tag{B2}$$

The velocity of the impacting ball is given by the time rate of change of the position of its center of mass, which is given by:

$$V = \frac{d\alpha}{dt} = \frac{d\beta}{dt} + \frac{du}{dt} \tag{B3}$$

Considering Impulse-Momentum relationship, we get:

$$V = V_0 - \frac{1}{m}\int_0^t F dt \tag{B4}$$

Using Eq. (B_3), we get

$$V_0 - \frac{1}{m}\int_0^t F dt = \frac{d\beta}{dt} + \frac{du}{dt} \qquad (B_5)$$

where F is the contact force between the ball and bar.

For a stress-wave uniformly distributed across the section of the cylindrical bar and traveling with velocity $C_0 = \sqrt{\frac{E}{\rho}}$, one obtains:

$$\frac{du}{dt} = \frac{F}{\rho C_0 A} \qquad (B_6)$$

where ρ is the density, A is the cross-sectional area, E is the modulus of elasticity, υ is Poisson's ratio of the bar, and C_0 is the wave velocity, which is equal to $\sqrt{\frac{E}{\rho}}$

The relationship between the contact force and the local deformation must now be specified. This is determined from classical Hertz contact theory (Timonshenko, 1982) and is given by:

$$F = K\beta^{3/2} \qquad (B_7)$$

where K is a constant dependent on the elastic and geometric properties of the contact surfaces. For the present case of a spherical ball in contact with a flat surface, K is given by

$$K = \frac{2}{3}\frac{E}{1-\upsilon^2} r^{1/2} \qquad (B_8)$$

Substituting Eqs. (B_6), (B_7) in (B_5) and differentiating with respect to time, we get a non-linear ordinary differential equation in terms of the variable β, which is a governing equation for impact against a rod.

$$\frac{d^2\beta}{dt^2} + \frac{K_2}{\rho C_0 a}\frac{d\beta^{3/2}}{dt} + \frac{K_2}{m}\beta^{3/2} = 0 \qquad (B_9)$$

As discussed in Chapter 2, the above equations were solved numerically for two cases with initial conditions:

$$\beta = 0, \quad V = V_0 \quad \text{at } t = 0$$

The following values for the constants were assumed (Barton, Volterra, Citron, 1958).

ρ=7.8gm/cm^3

ν=0.29

A= 5.067*10^5 cm/sec

C_0= 5.19*10^5 cm/sec

Three steel ball masses were considered. The first two were 538 and 67.5 grams (Barton, Volterra and Citron, 1958), corresponding to experimental ball diameters of 2 and 1 inches. The third mass was 345 grams used in the current experimental setup, corresponding to ball diameter of 1.7 inches. For each ball mass, four different impact velocities were considered, namely 242.61, 210.11, 171.52, and 121.30 cm/sec which corresponded to experimental height of drops of 30, 22.5, 15, and 7.5 centimeters. The results of these computations expressed under the form stress versus time were shown in Chapter 3, and also repeated here as Figs. B_1, B_2 and B_3, for completeness.

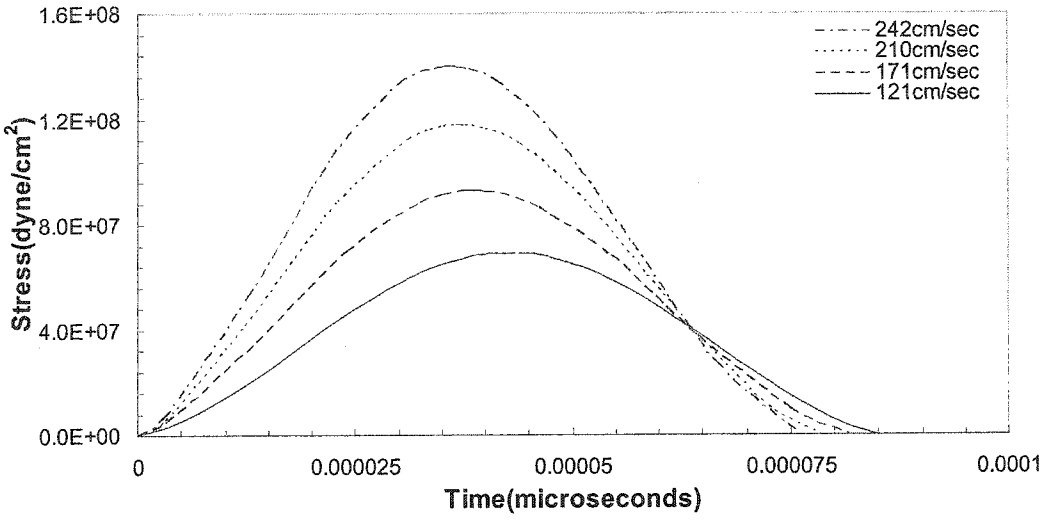

Fig.B_1 Stress versus time at the impact end of a 1 in. dia. bar impacted by a 1in. dia. ball at different impact velocities (Barton, Volterra and Citron, 1958)

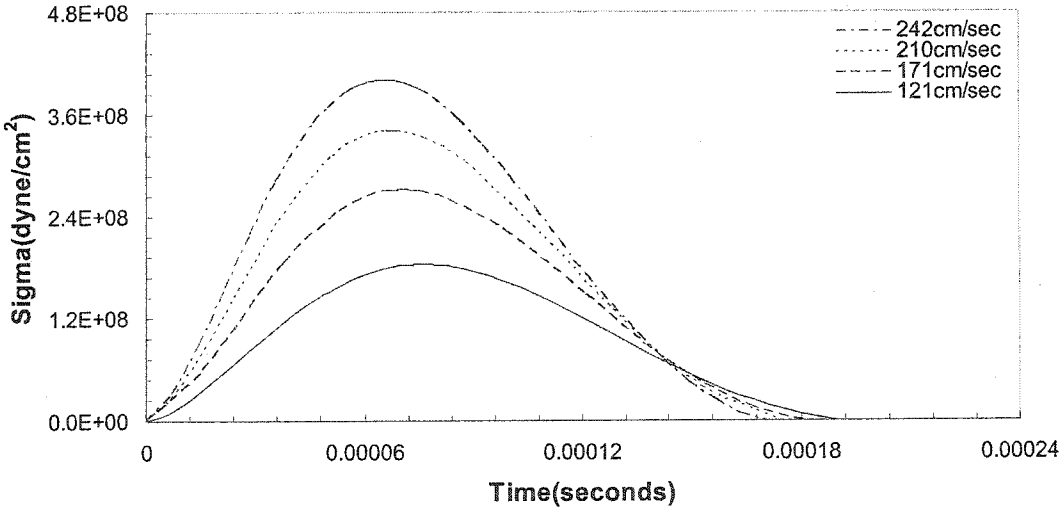

Fig.B_2 Stress versus time at the impact end of a 1 in. dia. bar impacted by a 2 in. dia. ball at different impact velocities (Barton, Volterra and Citron, 1958)

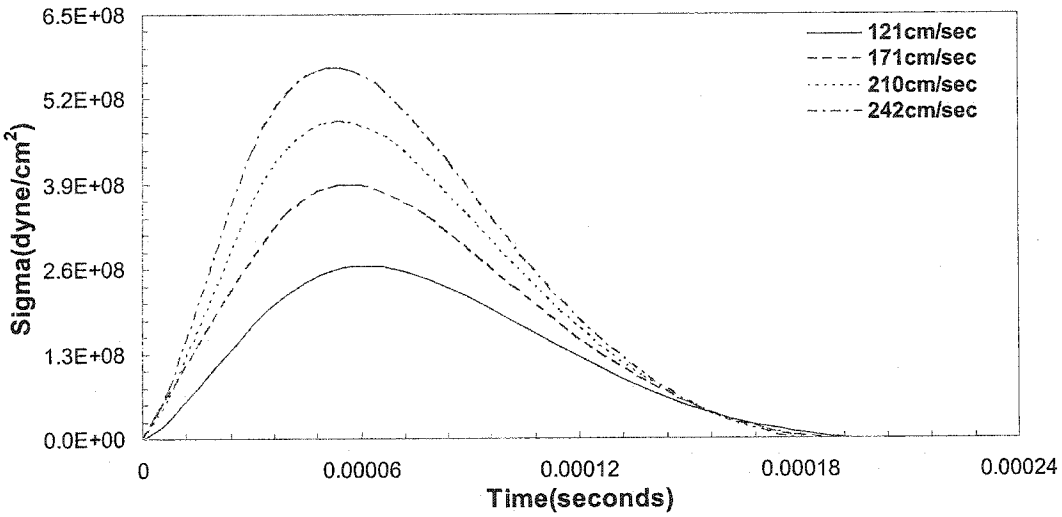

Fig.B$_3$ Stress versus time at the impact end of a 0.63 in. dia. bar impacted by a 1.7 in. dia ball at different impact velocities (current setup)

APPENDIX C

ILLUSTRATIONS OF CURRENT SHPB SETUP

The experimental setup consists of various important elements. The basic idea was to design and manufacture a frame in order to support the long cylindrical bars at various locations as well as to impact the input bar with a spherical ball at its center. The following are the important facts considered while designing the setup:

i. The frame employed should be a rigid one.

ii. The bars should be rested on supports that have very less frictional effects.

iii. Adjustable supports in order to facilitate the proper alignments of the bars.

iv. Certain mechanism that makes a spherical ball impact at the center of the input bar and allow it to rebound freely.

The basic components of SHPB setup shown in the following illustrations are:

1. Frame
2. Rotating Arm
3. Impacting ball & housing
4. Supports
5. Uniform steel input and output bars
6. Strain gauges

The frame consists of a 200 cm steel base consisting of a wooden plate and channel beams as shown in Fig. C_1, also visible are steel input and output bars supported on the wooden blocks grooved in to triangular shapes and also covered with Teflon.

The impacting ball and its housing supported with the rotating arm are viewed in the Fig. C_2. The spherical ball employed made of steel with diameter 4.2 cm, resting against two steel flanges held together using bolts and nuts. A rotating arm is used in order to support the ball housing freely, and to generate the energy required for impact. This arrangement for the loading was found to produce a smoothly increasing pulse followed by decreasing one (sinusoidal), as presented in Chapter 3.

Figure C_3 presents the full view of developed SHPB along with its instrumentation. As viewed in the figure electrical resistance strain gauges are attached to the input and output bars to monitor the traveling wave signals. The strain gages on the input bar sense the incident and reflected waves, whereas those on the output bar sense the transmitted wave.

The lead wires from the strain gauges on each bar were connected to a signal conditioner on multi channel amplifier. Three channels of the amplifier were used, two for the strain gage bridges on the input and output bars, and one for the triggering gages attached close to the impacted end of the input bar in a quarter bridge configuration.

The outputs from two amplifiers are fed to a two channels on Digital Storage Oscilloscope through BNC cables. Thus the incident, reflected and transmitted waves could be captured.

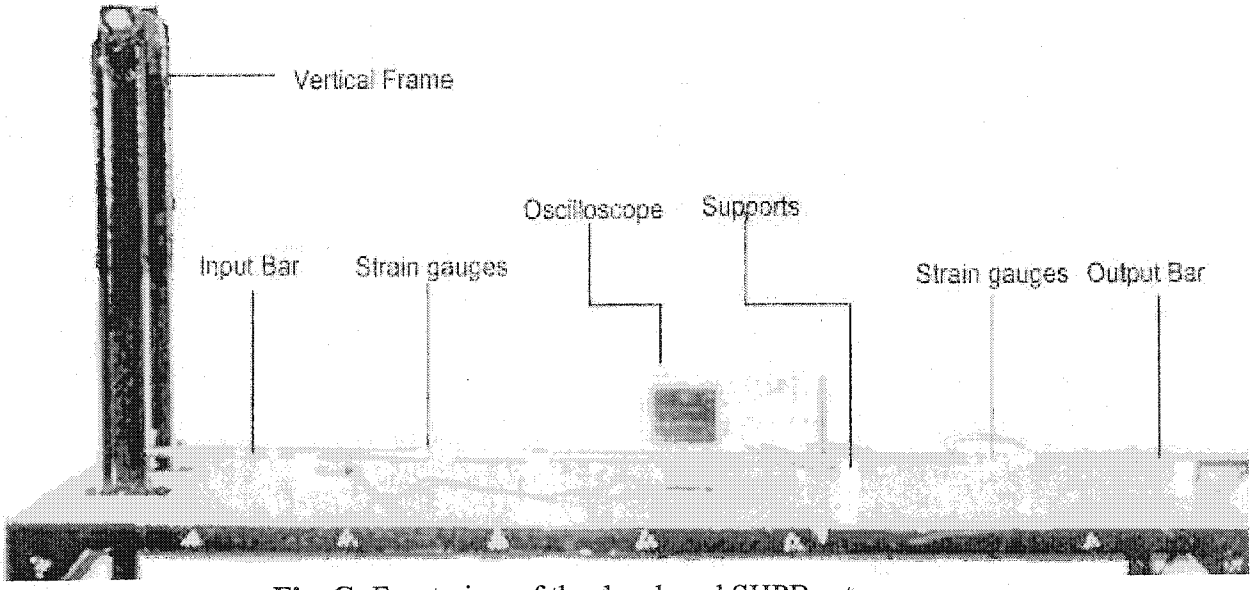

Fig. C_1 Front view of the developed SHPB setup

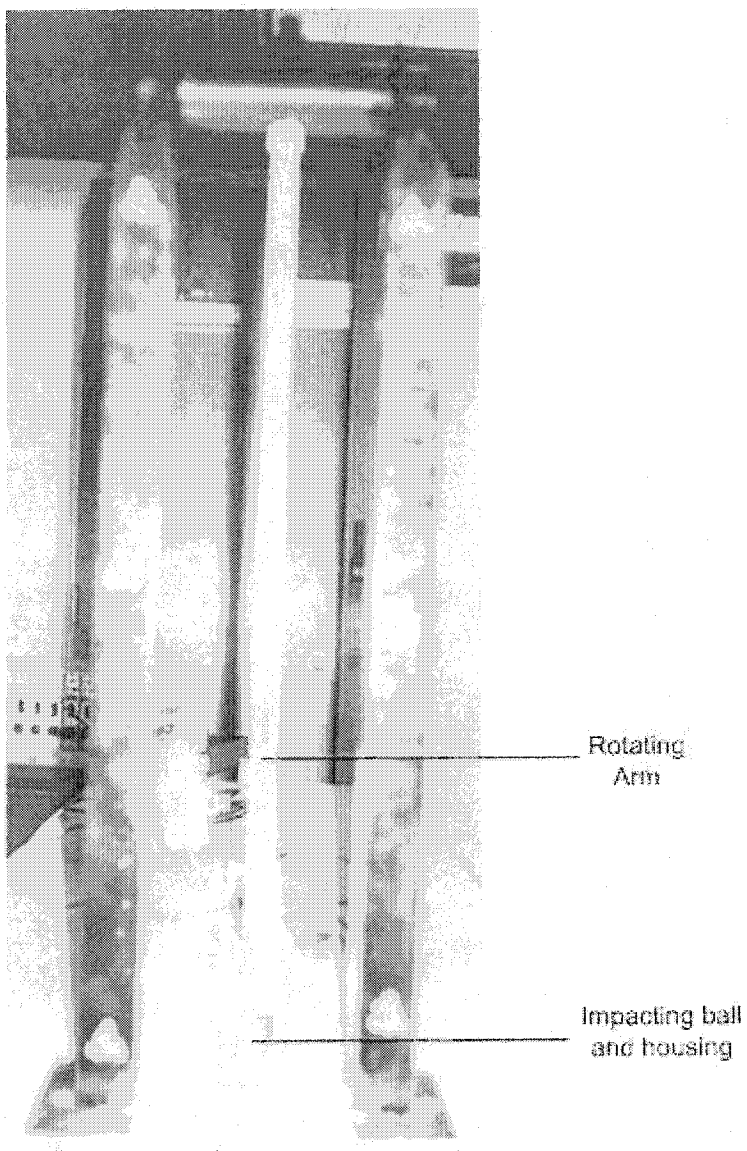

Fig. C_2 Side view of the developed SHPB setup

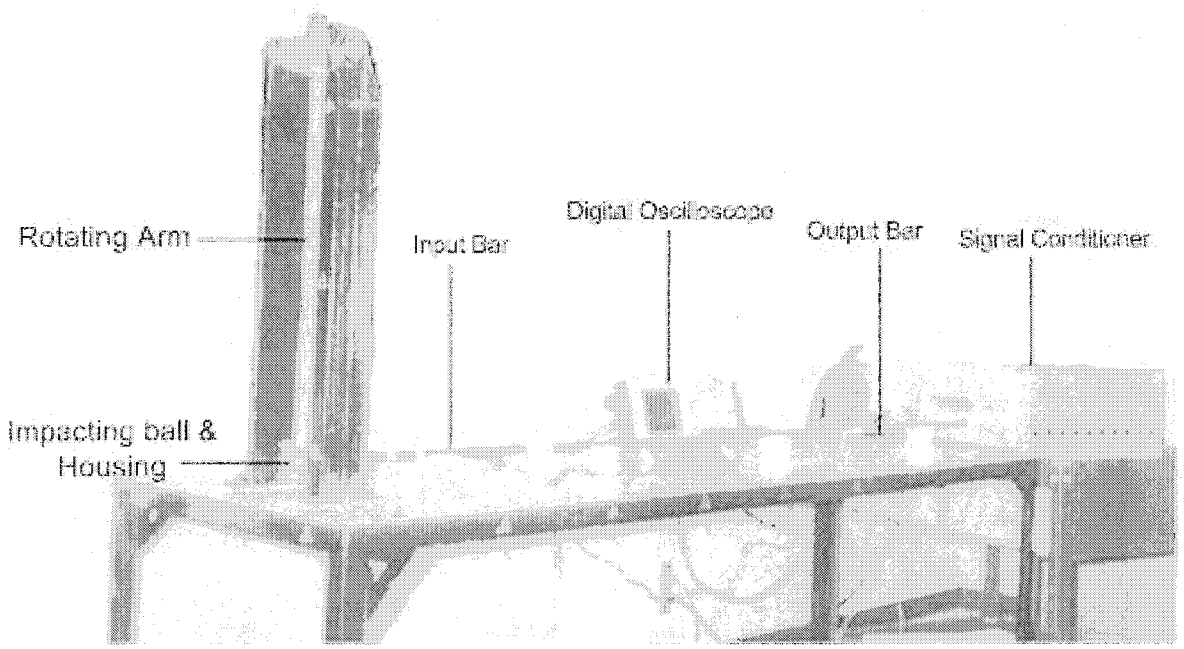

Fig. C_3 Full view of the developed SHPB setup

APPENDIX D

BACKGROUND ON ANSYS/LS-DYNA

The numerical simulation was performed using finite element software ANSYS/LS-DYNA. It has capability of solving large deformation dynamics, quasi-static and complex impact problems. The basic steps involved in this program are:

D-1 Building the Finite Element Model

The first step in an explicit dynamic analysis is to create the model that will represent the physical system to be analyzed. There are five basic ingredients in building a Finite Element Model, such as

i. Defining the element types and real constants

ii. Specifying material models

iii. Defining the model geometry

iv. Meshing the model

v. Defining contact surfaces

The ANSYS element library contains more than 150 different element types. Each element type has a unique number and a prefix that identifies the element category, such as BEAM4, PLANE77, SOLID96, etc. Therefore it is important to first set the Preferences options to "LS-DYNA Explicit" so that menus are properly filtered to show explicit dynamics input options only. Element types available for an explicit dynamic analysis are described briefly in Elements (ANSYS 6.1). More detailed descriptions of each explicit element can be found in the ANSYS\LS-DYNA element references.

Once the appropriate elements to represent the physical system are chosen, then the real constants that are associated with it are selected. One must determine which real constants (if any) are required for each element type included in the model.

After defining the element type for a model, its material properties will be specified. There are numerous material models available for use in an explicit dynamic analysis. One should refer to the element descriptions in the ANSYS element reference (ANSYS 6.1) to find out which material models are valid for a particular element. After deciding which material model (or models) to use in the analysis, one must define all of the properties associated with it. For some material models, one may use the EDCURVE command to define data curves associated with the material (e.g., a stress-strain curve).

After defining the element type and material properties, the geometry of the model is made. The easiest way to create the model geometry is with the solid modeling capabilities of the ANSYS program. For simple models (e.g., line elements only), one can use the direct generation modeling method. By this method, one can define the nodes and elements of the model directly.

After building the solid model, it is the time to mesh the model with nodes and elements. Meshing involves three main steps:

- Set the element attributes
- Set mesh controls
- Generate the mesh

To set the element attributes, one specifies previously defined element type, real constant set, and material property set to use for subsequent meshing.

Mesh controls allows to indicate the general size and shape of elements to use during meshing. There are numerous mesh controls available in the ANSYS program (*ANSYS Modeling and Meshing Guide*).

After specifying the desired mesh controls, the model has to be meshed.

An explicit dynamic analysis often includes contact between surfaces. After generating the Finite Element model, contact between the two separate surfaces will be applied. Defining contact involves four basic steps:

- Determine the type of contact which best defines the physical model
- Identify contact surfaces
- Specify friction coefficient parameters
- Specify additional input required for the chosen contact type

If automatic contact is not being used, contact surfaces are defined by grouping the nodes on each surface into a component. Once these components are created, the contact between the desired surfaces (i.e., node components) is then specified along with its coefficient of friction.

D-2 Application of Loads and Obtaining Solution

After building the model, the next step is to apply loads to the structure in preparation for solution. In order to properly model the structure behavior, it is necessary to apply loads with respect to a specified time interval. Unlike most implicit analyses, all loads in an explicit analysis must be time-dependent in nature. Hence, when using ANSYS/LS-DYNA, many of the standard ANSYS commands are not valid. In particular, the F, SF, and BF family of commands are not applicable in ANSYS/LS-DYNA because they can only be used to specify time-independent loads. Additionally, the D command

can only be used to define constrained nodes. For this reason, all loads in ANSYS/LS-DYNA are applied using a pair of array parameters, one corresponding to the time and the other corresponding to the loading condition.

In ANSYS/LS-DYNA, all loads are applied in one load step. This is much different from an implicit analysis where loads are often applied in multiple steps. In ANSYS/LS-DYNA, for certain kinds of loads, one can also specify when a load is imposed on a body (birth time), and when the load is removed (death time).

To apply a load to the model, one needs to follow these steps:

- Designate portions of the model that will receive the load as components (or parts, for rigid bodies)
- Define array parameters containing time intervals and load data values
- Specify load curves
- Define the load direction if the load is not acting in the global coordinate system
- Apply loads to the model

After the model has been built (i.e., after completing element definitions, real constant and material property specifications, modeling, meshing, boundary/initial conditions, loading, and termination controls), one can start the solution process.

When the solution is complete without errors or warnings, the ANSYS/LS-DYNA GUI notifies the user that the solution is done, and control is transferred back to the ANSYS/LS-DYNA program. The results can be viewed using the POST1 and POST26 processors of the ANSYS/LS-DYNA program.

The point at which the LS-DYNA solution terminates will depend on the termination controls one specifies when setting up the model. Several types of termination controls are available:

- Termination time - Use the TIME command to specify an end-time for the analysis. The calculation will stop when the accumulation of time steps reaches that end-time.
- CPU time limit – One can specify the CPU time limit (in seconds). The calculation will stop when that time limit is reached.
- Termination criteria – The solution can be stopped by giving certain end criteria, such as, when a specific node or rigid body reaches a certain position, or when a specific node comes into contact with another surface.

One should always specify an analysis end-time using the TIME command. The other termination controls are optional. The solution will terminate when any one of the specified termination criteria are met.

D-3 Reviewing the Results

ANSYS/LS-DYNA results can be reviewed using the two ANSYS postprocessors, POST1 and POST26. POST1 is used to view results for the entire model at specific time points, or to view animated results. POST26 is used to view the results of a specific component of the model at a larger number of time points over a period of time. With an explicit dynamic analysis, one will typically want to view animated results (POST1) and time-history results (POST26). Details of POST1 and POST26 are given in the user guide (ANSYS 6.1).

Vitae

- MAHMOOD, SYED IFTEKHAR
- Born at Hyderabad, India in 1978.
- Received Bachelor of Engineering (B.E.) degree in Mechanical Engineering from Osmania University, Hyderabad India in 2000
- Received Master of Science (M.S.) degree in Mechanical Engineering from King Fahd University of Petroleum & Minerals, Dhahran, Saudi Arabia in 2004.